International Journal of Nanomedicine

Dovepress
Taylor & Francis Group

Open Access Full Text Article

ORIGINAL RESEARCH

Antibiofilm and Anticancer Activity of Multi-Walled Carbon Nanotubes Fabricated with Hot-Melt Extruded Astaxanthin-Mediated Synthesized Silver Nanoparticles

Han-Sol You[1,*], Young-Sun Jang[2,*], Anbazhagan Sathiyaseelan[1], Su-Ji Ryu[1], Ha-Yeon Lee[1], Jong-Suep Baek[1,3]

[1]Department of Bio-Health Convergence, Kangwon National University, Chuncheon, 24341, Republic of Korea; [2]College of Pharmacy, Kangwon National University, Chuncheon, 24341, Republic of Korea; [3]BeNatureBioLab, Chuncheon, 24206, Republic of Korea

*These authors contributed equally to this work

Correspondence: Jong-Suep Baek, Email jsbaek@kangwon.ac.kr

Purpose: Multi-walled carbon nanotubes (MWCNTs) were used as carriers for silver nanoparticles (AgNPs). In this process, MWCNTs were coated with mesoporous silica (MWCNT-Silica) for uniform and regular loading of AgNPs on the MWCNTs. In addition, astaxanthin (AST) extract was used as a reducing agent for silver ions to enhance the antioxidant, antibiofilm, and anticancer activities of AgNPs. In this process, AST was extracted from *Haematococcus pluvialis (H. pluvialis)* and processed by hot melt extrusion (HME) to enhance the AST content of *H. pluvialis*. AST has strong antioxidative properties, which leads to anticancer activity. In addition, AgNPs are well known for their strong antibacterial properties. The antibiofilm and anticancer effects were studied comprehensively by loading the AST AgNPs onto MWCNT-Silica.

Methods: AgNPs-loaded MWCNT-silica (MWCNT-Ag) was prepared through the binding reaction of TSD and silanol groups and the aggregation interaction of Ag and TSD. To enhance the antioxidant, antibiofilm, and anticancer activities of AgNPs, HME-treated *H. pluvialis* extract (HME-AST) was used as a reducing solution of silver ions. The increased AST content of HME-AST was confirmed by high-performance liquid chromatography (HPLC) analysis, and the total phenol and flavonoid content analysis confirmed that HME enhanced the active components of *H. pluvialis*. The antibiofilm activity of MWCNT-AST was investigated by biofilm inhibition and destruction test, SEM, and CLSM analysis, and the anticancer activity was investigated by WST assay, fluorescent staining analysis, and flow cytometry analysis.

Results: MWCNT-AST showed higher antioxidant activity and antibiofilm activity than MWCNT-Ag against *E. coli, S. aureus*, and methicillin-resistant *S. aureus* (MRSA). MWCNT-AST showed higher anticancer activity against breast cancer cells (MDA-MB-231) than MWCNT-Ag, and lower toxicity in normal cells HaCaT and NIH3T3.

Conclusion: MWCNT-AST exhibits higher antioxidant, antibiofilm, and anticancer activities than MWCNT-Ag, and exhibits lower toxicity to normal cells.

Keywords: *Haematococcus pluvialis*, astaxanthin, silver nanoparticles, multi-walled carbon nanotubes, anticancer, antibiofilm, multi-drug resistance

Introduction

The beneficial effects of microalgae components and their biological properties such as antioxidant and anticancer properties are being studied.[1–4] Among these, *Haematococcus pluvialis* (*H. pluvialis*) is considered one of the most important microalgae as a source of astaxanthin (AST).[5] *H. pluvialis* contains many bioactive compounds such as carotenoids, proteins, lipids, carbohydrates, and other substances.[5] AST (3,3'-dihydroxy-β, β'-carotene-4,4'-dione) is one

Received: 29 August 2024
Accepted: 11 December 2024
Published: 8 January 2025

Graphical Abstract

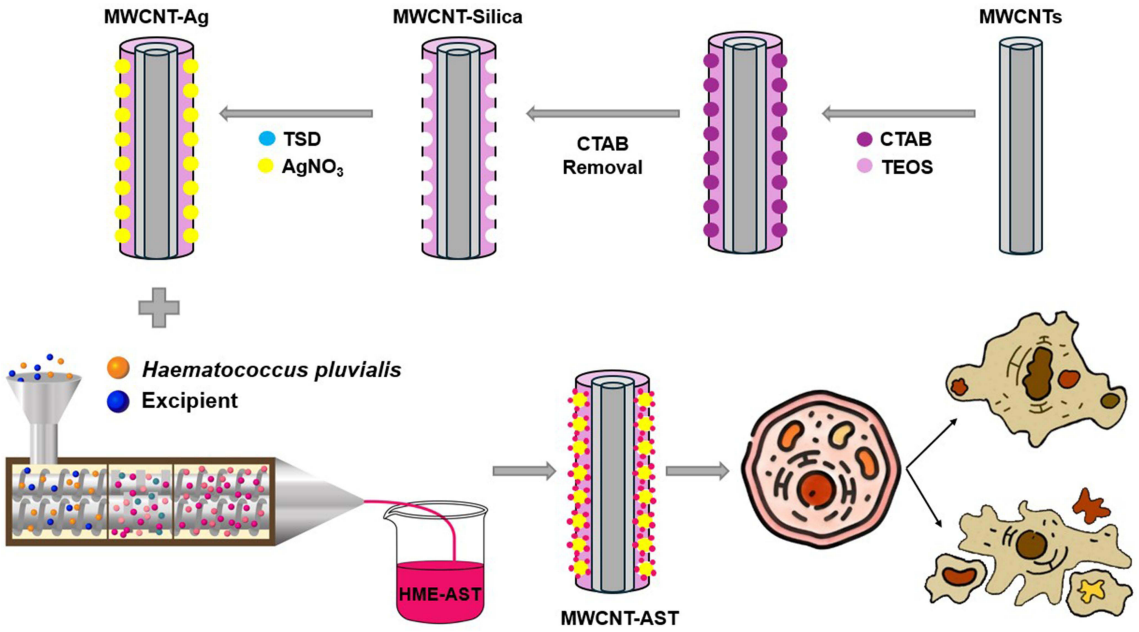

of the xanthophyll carotenoids.[6] AST, the main carotenoid produced in aquaculture, has the highest oxygen radical absorption capacity compared to other carotenoids.[7,8] It has also been reported to have a much higher antioxidant capacity than α-tocopherol (vitamin E),[9] inhibits mitochondrial lipid peroxidation, and contributes to the inhibition of cell membrane peroxidation.[10,11] As interest in products made from biological raw materials increases, the natural AST market is forming, but it is a very small percentage compared to the synthetic AST market. Chemically synthesized AST has lower antioxidant efficacy than natural AST and is not yet approved for human consumption.[12,13] However, the amount of AST contained in *H. pluvialis* is very small, 1–5%.[5] We suggest Hot melt extrusion (HME) as a method to increase the content of AST from *H. pluvialis*.

HME has been proven as an effective technology in various fields, including its utilization in pharmaceutical formulations, for improving the solubility of hydrophobic substances, target delivery, drug release, and the production of nanoparticles (NPs).[14,15] The advantage of HME lies in its eco-friendly nature, as it eliminates the need for organic solvents. Moreover, it promotes the dispersion of drugs and enhances the solubility of poorly soluble compounds, thereby increasing their bioavailability.[15] Furthermore, incorporating suitable additives during HME processing can imbue distinct characteristics to the final product through the extrusion process.[16,17] Ascorbyl palmitate serves as a bio-friendly antioxidant in the food industry.[18] Hydroxypropyl methylcellulose (HPMC) polymer is frequently used to manufacture sustained-release matrix systems due to its high safety and ease of use.[19] Lecithin, when used as an emulsifier, increases the ability of an active ingredient to dissolve by improving its dissolution.[20] Previous studies have reported that the extraction yield of microalgae components can be increased using the extrusion process.[21]

Silver nanoparticles (AgNPs) synthesized via components extracted from microalgae are continuously being studied.[22–24] Pigments, polysaccharides, peptides, and enzymes present in cell extracts or supernatants can reduce silver ions to nanoparticles.[25,26] Biomolecules contained in microalgae are responsible for the reduction of silver ions and can also act as capping agents to prevent aggregation, reduce toxicity, and increase the stability of nanoparticles.[27] Astaxanthin can scavenge free oxygen radicals, and AST extracted from *H. pluvialis* exhibits higher antioxidant activity than synthetic AST.[28] In addition, AST exhibited anticancer activity against bladder cancer, colon cancer, oral cancer, and breast cancer.[29–32] AgNPs are proposed as one of the treatments for biofilms of bacteria and multidrug-resistance (MDR)

bacteria.[33–37] In recent times, the utilization of nanoparticles (NPs) has markedly broadened across diverse domains. NPs have proven efficacious in medical and pharmaceutical nanoengineering, particularly for facilitating therapeutic drug transport.[38] Additionally, AgNPs have been reported to have the ability to reduce microbial infections on the skin.[39] The antibacterial effectiveness of AgNPs stems from their unique physicochemical properties, such as their nanometer-scale size, elevated surface area, mass ratio, and heightened reactivity.[40,41] These previous studies suggest that using HME-processed *H. pluvialis* extracts as a reducing agent for AgNPs can alleviate toxicity to normal cells while enhancing antioxidant, antibiofilm, and anticancer activities.

Biofilms are a serious health issue due to their ability to confer MDR capacity, host defenses, and other stresses.[42] Biofilms are complex three-dimensional assemblies of bacteria, attached to surfaces and flexibly embedded in an extracellular polymeric substance (EPS) matrix. These biofilms form on all substrates and associated infections in plants, animals, and humans.[43–45] Infections caused by *Staphylococcus aureus* (*S. aureus*) cost $4 billion annually in treatment and care costs in America.[46] According to the National Institute of Health, the main cause of pathogenic infections in humans is the formation of biofilms, which account for more than 80% of infections.[47] The rise of MDR microorganisms is a global threat to human health.[33] Bacteria exposed to antibiotics can develop resistance to the antibiotic and transmit this resistance to other microorganisms. In addition, even if it is a different drug, antibiotics with the same structure may develop resistance to it, resulting in the development of MDR bacteria.[37] Research is ongoing to develop inhibitors of the bacterial biofilms responsible for these human health problems and treatments for antibiotic-resistant bacteria.

Cancer, a type of disease caused by uncontrolled cell growth, is classified into carcinomas, sarcomas, lymphomas, leukemias, germ cell tumors, and blastomas, depending on the presumed origin of the tumor cells.[48] Among them, carcinoma refers to cancer originating from epithelial cells and includes breast cancer.[49] Breast cancer is the most common type of cancer in women, accounting for almost 30% of all cancers.[50] If diagnosed early, treatment is possible, but after metastasis, it can spread through the blood and lymphatic system, making treatment difficult and increasing mortality. Existing cancer treatments include chemotherapy, radiotherapy, and surgery, but these methods cause normal tissue damage, multidrug resistance, toxicity, and side effects.[51] To overcome these problems, methods of using natural products as anticancer agents are being studied.[52] Nanoparticles (NPs) synthesized from plant extracts, which are under constant research, can improve the bioavailability of natural products in cancer treatment.[53] Other studies have demonstrated the anticancer activity of AgNPs synthesized from plant extracts.[54–56] However, the high cytotoxicity of AgNPs has many limitations in cancer treatment because it kills not only cancer cells but also normal cells.[57]

Materials containing AgNPs are superior to existing antibacterial materials because they can release silver ions slowly over a long period, resulting in high safety and stability and long-lasting antibacterial activity.[58] Zeolite, calcium phosphate, silica, and mesoporous materials have been reported as carriers for producing silver-containing antibacterial materials.[59–63] Mesoporous silica is known to be a very suitable medium for drug delivery and nanoparticle transport due to its tunable pore size, large surface area, various functionalizations, and excellent biocompatibility.[64,65] Carbon nanotubes (CNTs) are one-dimensional carbon nanomaterials that are divided into single-walled carbon nanotubes (SWCNTs) made of a single graphite layer and multi-walled carbon nanotubes (MWCNTs) made of multiple coaxial layers.[66] Previous reports have demonstrated that antibiofilm activity can be increased by using MWCNTs as a carrier for drugs.[67] It has been reported that combining AgNPs with MWCNTs can exhibit superior antibacterial properties compared to simple MWCNTs.[68] Another study reported that AgNPs combined with MWCNTs had higher antibacterial activity against *Escherichia coli* (*E. coli*) than simple MWCNTs.[69] However, MWCNTs are easily aggregated in aqueous solutions due to their high aspect ratio and low hydrophilicity, which makes it difficult to use them as drug carriers.[70] Stable CNTs dispersion can be achieved by using surfactants such as hexadecyl trimethyl ammonium bromide (CTAB), octyl phenol ethoxylate (Triton X-100), and sodium dodecyl sulfate (SDS).[71–73] In addition, mesoporous silica coating can improve the dispersion of MWCNTs in aqueous solution.[74,75]

We suggested that using AST extract as a reducing agent for silver ions could increase the antioxidant, antibiofilm, and anticancer activities of MWCNTs decorated with AgNPs. We produced AST by HME treatment of *H. pluvialis*. We developed the MWCNT-AST by loading AST AgNPs synthesized from AST extract on mesoporous silica-coated MWCNTs. MWCNT formulations were assessed for biofilm inhibition and destruction activity against *E. coli,*

S. aureus, and methicillin-resistant *S. aureus* (MRSA) and anticancer activity against human breast cancer cells MDA-MB-231.

Materials and Methods

Materials

Haematococcus pluvialis (H. pluvialis) was provided by Chonbuk National University (Iksan, Korea). Cetyltrimethylammonium bromide (CTAB), sodium hydroxide (NaOH), Ammonium nitrate (NH_4NO_3), and silver nitrate ($AgNO_3$) were purchased from Daejung Chemical (Siheung, Korea). MWCNT, Tetraethyl Orthosilicate (TEOS), and N-[3-(trimethoxysilyl) propyl] ethylene diamine (TSD) were purchased from the Tokyo chemical industry (TCI,Tokyo, Japan). *Escherichia coli* (ATCC 43888), *Staphylococcus aureus* (ATCC 19095), and Methicillin-resistant *Staphylococcus aureus* (ATCC 43300) were purchased from the American Type Culture Collection (ATCC). MDA-MB-231, HaCaT, and NIH3T3 cells were purchased from the Korea Cell Line Bank (Seoul, Korea). Mueller Hinton Broth (MHB) was purchased from Kisanbio (Seoul, Korea). Water-soluble tetrazolium (WST)-1 assay kit (EZ-CyTox, Daeil Lab Service), Fetal bovine serum (FBS), penicillin and streptomycin (P/S), Dulbecco's modified eagle medium (DMEM) were procured from Thermo Fisher Scientific (Massachusetts, USA). Propidium iodide (PI), rhodamine 123 (Rh123), ethyl bromide (EB), and acridine orange (AO) were brought from Sigma-Aldrich (St. Louis, USA). Annexin V-FITC, PI, and Calcein-AM were brought from Invitrogen (Waltham, Massachusetts, USA).

Manufacture of AST Formulations Through HME Processing

H. pluvialis was loaded into a twin-screw extruder (STS25-28FD, co-rotating intermeshing type twin-screw extruder, Pyeongtaek, Korea). The temperature profile from the feed zone of the extrusion mold to the injection die was 60°C. After the HME process was completed, the extrudate was dried in an oven (SCOV-150, Sungchan Science, Pocheon, Korea) at 60°C for 12 hours, and the ground powder was stored for later experiments. The compositions of HME-treated AST and biopolymers are shown in Table S1.

Determination of AST in Formulations

To select the formulation to be used for MWCNT-AST synthesis from the manufactured AST formulations, the AST content and total phenol contents (TPC) and total flavonoid contents (TFC) were measured by HPLC analysis. The analytical conditions of HPLC are shown in Table S2. The total phenol and flavonoid contents were performed in the same manner as in section TPC and TFC.

Preparation of MWCNT-Silica

MWCNT-Silica was synthesized using a slightly altered procedure from previous research.[76] The chemical compositions of the MWCNT formulations are shown in Table 1. 30 mg of MWCNTs were placed in 30 mL CTAB solution of 137 mM and ultrasonicated in a sonic bath for 3 hours and tip ultrasonicated in an ice bath for 1 hour. Afterward, it was diluted with 100 mL of distilled water, adjusted to basicity by adding 0.3 mL NaOH solution of 2M, and preheated at 60°C for 10 minutes. 7.5 mL of TEOS solution diluted with ethanol was added dropwise while stirring and reacted at

Table 1 Preparation of various MWCNT Formulations

MWCNT	MWCNT-Silica	MWCNT-TSD	MWCNT-Ag	MWCNT-AST 1	MWCNT-AST 5	MWCNT-AST 10
• MWCNT	• MWCNT • CTAB • TEOS	• MWCNT • CTAB • TEOS • TSD	• MWCNT • CTAB • TEOS • TSD • $AgNO_3$	• MWCNT • CTAB • TEOS • TSD • $AgNO_3$ • AST F2 (1 mg/mL)	• MWCNT • CTAB • TEOS • TSD • $AgNO_3$ • AST F2 (5 mg/mL)	• MWCNT • CTAB • TEOS • TSD • $AgNO_3$ • AST F2 (10 mg/mL)

Abbreviations: MWCNT, Multi-walled carbon nanotube; CTAB, Cetyltrimethylammonium bromide; TEOS, Tetraethyl orthosilicate; TSD, N-[3-(trimethoxysilyl) propyl] ethylene diamine; $AgNO_3$, Silver nitrate; AST, Astaxanthin.

60°C for 12 hours. Afterward, the mixture was centrifuged to obtain a pellet, which was washed with NH_4NO_3 ethanol solution (12.5 mM) in a sonic bath for 2 hours, and this was repeated three times to prepare MWCNT-Silica.

Preparation of MWCNT-TSD, MWCNT-Ag, and MWCNT-AST

AgNPs-decorated MWCNT-Silica (MWCNT-Ag) was prepared by referring to the previous method.[75] To prepare MWCNT-Ag, 60 mM $AgNO_3$ aqueous solution and TSD solution diluted with ethanol were mixed at a molar ratio of 1:1. Then, 20 mg of MWCNT-Silica and 0.96 mL of $AgNO_3$/TSD solution were added to 11.04 mL of ethanol. MWCNT-TSD was prepared by adding only 0.96 mL of TSD solution. After sonicating for 30 minutes, the mixture was stirred at 60°C for 3.5 hours. Afterward, the pellet was collected by centrifugation and washed three times with ethanol to prepare MWCNT-Ag. For the MWCNT-AST preparations, 0.96 mL of $AgNO_3$/TSD solution was added and stirred at 60°C for 2 hours, then AST extracts of each concentration were added and stirred for 1.5 hours, and the pellet was collected and washed. The concentration of the AST extract was selected from a previous study.[74]

Characterization of MWCNT Formulations

To observe physical properties, MWCNT formulations were analyzed using Transmission electron microscopy (TEM) equipped with an energy-dispersive spectroscope (EDS) (JEM-2100F, JEOL, Tokyo, Japan) and Scanning Electron Microscopy (SEM) (S-4800, Hitachi, Japan). Polydispersity index (PDI), and particle size were measured using a Dynamic light scattering (DLS) (Zetasizer Nano ZS, Malvern Instruments, Malvern, UK). Zeta potential was measured using an Elastic Light Scattering (ELS) (Zetasizer Nano ZS, Malvern Instruments, Malvern, UK). Samples were dispersed in distilled water to prepare them for DLS and ELS measurements. The chemical compositions of AST and the MWCNT formulations were analyzed with a Fourier-Transform Infrared Spectroscopy (FT-IR) spectrometer (Nicolet iN10, Thermo Fisher Scientific, Waltham, MA, USA) in the range of 400–4000 cm^{-1}. An X-ray diffractometer (XRD) (X'pert-pro MPD, PAN analytical, Netherland) was used to investigate the XRD pattern of the MWCNT formulations at a 2θ ranging from 5° to 80°. Thermal gravimetric analysis (TGA) was performed using a Thermal Analysis system (SDT650, TA Instruments, USA). Raman spectroscopy analysis was performed using the RAMAN touch (Nanophoton Corporation, Japan) instrument.

Total Phenol Contents (TPC)

TPC was performed with slight modifications from the previous method.[15] 50 μL of the sample, 200 μL of 7.5% sodium carbonate, 250 μL of Folin-Ciocalteau reagent, and 700 μL of distilled water were mixed in a test tube. After reacting for 45 minutes in dark conditions at room temperature, absorbance was measured at 760 nm. The total phenol content of each formulation was calculated from a standard curve of gallic acid.

Total Flavonoid Contents (TFC)

125 μL of sample, 375 μL of ethanol, 25 μL of 10% aluminum chloride hexahydrate, 25 μL of 1M potassium acetate, and 700 μL of distilled water were placed in a test tube. After reacting in the dark for 40 minutes, absorbance was measured at 425 nm. Total flavonoid content was calculated from the standard curve of quercetin.[77]

Antioxidant Activity

7.4 mM ABTS solution and 2.4 mM potassium persulfate were mixed 1:1 and reacted in the dark for 16 hours. The ABTS solution was diluted with distilled water and adjusted to show an absorbance value of 0.7 at 734 nm. 100 μL of sample and 100 μL of ABTS solution were added to a 96 well plate and reacted for 20 minutes in the dark. In the DPPH assay, 0.1 mM DPPH methanol solution 100 μL and sample 100 μL in the dark for 20 minutes. The absorbance was measured at 734 and 517 nm to obtain the IC_{50} value of each sample.[75]

Biofilm Inhibition and Destruction Test

E. coli, S. aureus, and MRSA were adjusted to an absorbance of 0.1 at OD 600 nm using an MHB medium. To evaluate biofilm inhibition activity, 100 μL of sample and 100 μL of bacterial suspension were added to a 96 well plate and incubated

at 37°C for 24 hours. Distilled water was used as a negative control. To evaluate biofilm destruction activity, 100 μL of bacterial suspension was placed in a 96 well plate and incubated statically in a 37°C incubator for 24 hours. The bacterial suspension was then removed and 100 μL of sample was added. Afterward, the plate was incubated at 37°C for 24 hours. After incubation, the suspension was deleted, and the plates were washed with 100 μL of PBS and dried for 30 minutes at room temperature. Biofilms were stained by adding 200 μL of 0.1% v/v crystal violet. After 20 minutes, the plate was washed with water and dried at room temperature. To elute the stained bacteria, 200 μL of ethanol was added and kept at room temperature for 30 minutes. Afterward, the inhibition and destruction rate was calculated by measuring the absorbance at OD 600 nm.[78]

Microscopic Analysis of MRSA Biofilm

MRSA cultured in MHB medium was diluted to 10^8 cfu/mL mixed 1:1 with the sample and then incubated at 37 °C for 24 hours. After incubation, MRSA was collected by centrifugation at 5,000 rpm for 10 minutes. The collected bacterial cells were washed with PBS and resuspended in 1 mL of PBS. Then, 10 μL of Calcein-AM and PI (1:1 ratio) solution was added to the MRSA suspension and incubated at room temperature in the dark for 15 minutes. A drop of the stained MRSA suspension was placed on a confocal dish and observed under a Super Sensitive High-Resolution Confocal Laser Scanning Microscope (CLSM) (LSM880 with Airyscan, Carl Zeiss, Germany).[79]

Scanning Electron Microscope (SEM) Analysis

MRSA was cultured in MHB medium at 37 °C for 24 hours. MRSA diluted to 10^8 cfu/mL was mixed 1:1 with the sample and cultured for 24 hours. MRSA was collected by centrifugation at 5,000 rpm for 10 minutes and washed with PBS. After fixation with 2.5% glutaraldehyde, it was washed with PBS. Afterwards, it was dehydrated with 30, 50, 70, and 90% ethanol, dried, and analyzed.[80]

Cytotoxicity

A breast cancer cell line (MDA-MB-231), a normal mouse skin cell line (NIH3T3), and a normal human skin cell line (HaCaT) were grown in DMEM supplemented with 10% FBS and 1% P/S at 37°C with 5% CO_2. Cytotoxicity was determined by WST assay. Briefly, MDA-MB-231, NIH3T3, and HaCaT cells were seeded into a 96 well plate at a density of 2×10^4 cells/well. They were incubated for 24, 48, and 72 hours. After incubation, 10 μL of the diluted sample for each concentration was added to each well and cultured for 24, 48, and 72 hours. Then, 10 μL of WST solution was added to each well and incubated for 1 hour, and the absorbance was measured at OD 450 nm.[81]

$$\text{Cell viability}(\%) = A_{\text{sample}} / A_{\text{control}} * 100$$

Fluorescent Staining Analysis

MDA-MB-231 cells were seeded in 12 well plates and incubated for 24 hours at 37°C with 5% CO_2. MWCNT-Ag and MWCNT-AST 10 were treated and incubated for 24 hours at 37°C with 5% CO_2. Cells were stained using AO/EB, Rh123, and PI reagents and detected by fluorescence microscopy.[82]

Flow Cytometry Analysis

Flow cytometry was used to analyze apoptosis in MDA-MB-231 cells using Annexin V-FITC and PI.[83] Cells were seeded in 6 well plates and cultured until grown to 90% density. Samples were treated at 250 μg/mL and incubated at 37°C with 5% CO_2. After 24 hours, cells were recovered, washed, and stained with Annexin V-FITC and PI for analysis.

Statistical Analysis

The data was presented as mean ± standard deviation. The statistical significance was determined by a three-way analysis of variance (ANOVA). The p-value of <0.05 was considered statistically significant.

Results

Determination of AST in Formulations

In HPLC analysis, almost no AST content was detected in *H. pluvialis* without HME treatment (Figure S1). A significantly increased AST content was confirmed in AST formulations treated with HME. AST F2 and AST F3 showed much higher AST contents than AST F1. This is suggested by the effect of HPMC added during the HME process. HPMC, a nonionic component of water-soluble cellulose ether derivatives, can improve the water solubility and bioavailability of the material.[84,85] Measurements of total phenol and flavonoid content showed that the control had very low content. Additionally, the flavonoid content of AST F1 hardly increased, and phenol increased slightly, but not significantly. AST F2 and AST F3 showed higher phenol and flavonoid content than AST F1. AST F2 showed significantly increased phenol and flavonoid content than AST F3. This is thought to be influenced by the increased AST content confirmed in the HPLC results. Based on these results, it was decided to use AST F2 for MWCNT-AST synthesis.

Characterization of MWCNT Formulations

TEM Analysis

The morphological characteristics of the MWCNT preparation and the size and dispersion of the AST AgNPs loaded into the MWCNT were confirmed (Figure 1A). As a result of the comparative analysis of MWCNT-Ag, MWCNT-AST 1, and MWCNT-AST 5, the size of the AgNPs contained in the MWCNT-Silica was found to be small. However, in the case of MWCNT-AST 10, it was confirmed that the size of the particles loaded on the MWCNT increased, but the dispersibility of the particles was high and the particle formation was found to be uniform. The presence and distribution of silver ions contained in the MWCNTs were confirmed by EDS mapping (Figure 1B). The amount of silver ions contained in the MWCNTs was confirmed through the EDS spectrum (Figure S2). MWCNT-AST was found to be more uniform and to have a higher Ag ion content compared to MWCNT-Ag. These results suggest that the AST extract helps to reduce silver ions and forms more uniform and higher amounts of AgNPs on MWCNTs. In a previous study, it was confirmed that the

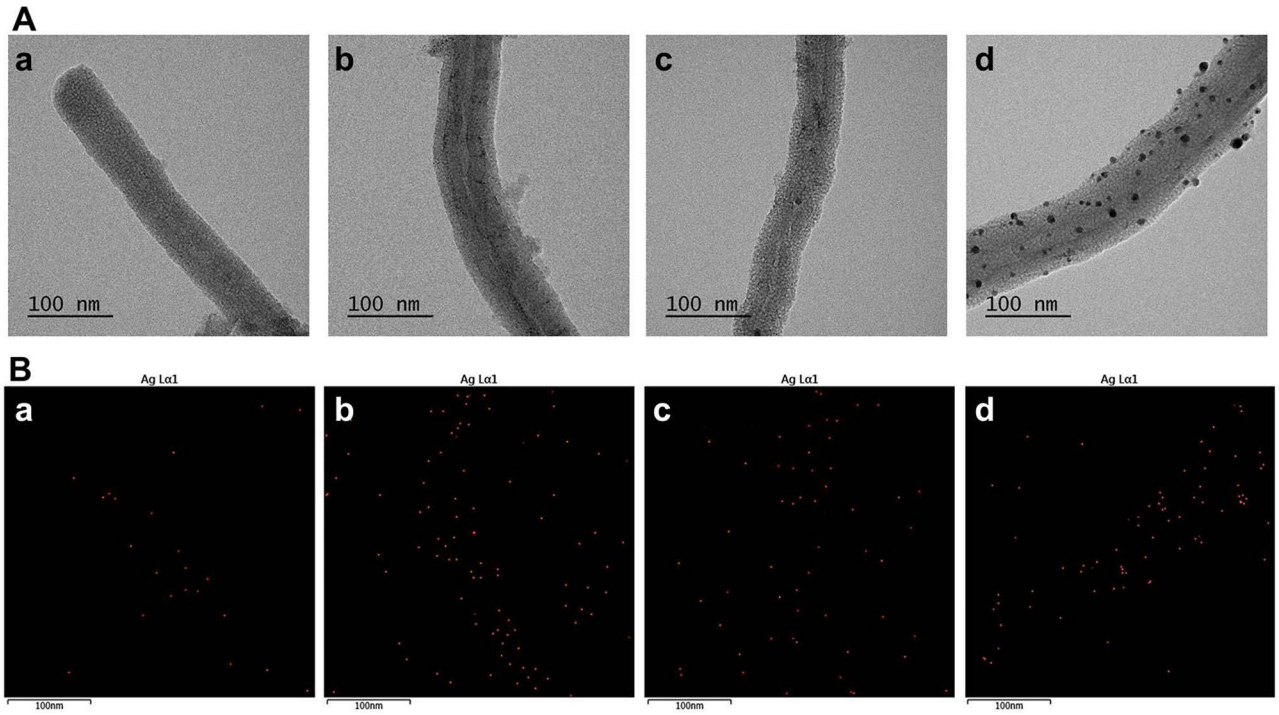

Figure 1 (**A**)TEM image of various MWCNT formulations and (**B**) EDS mapping of Ag in MWCNT formulations. (a) MWCNT-Ag; (b) MWCNT-AST 1; (c) MWCNT-AST 5; (d) MWCNT-AST 10.

https://doi.org/10.2147/IJN.S485722

mesoporous silica coating did not change the shape of MWCNTs, and the addition of TSD for Ag binding also did not change the shape of MWCNTs and MWCNT-Silica.[75,86]

SEM Analysis

SEM analysis was performed to investigate the surface properties of the MWCNT formulations. The pure MWCNTs exhibited a cylindrical shape with a length of approximately 1 μM, and the thickness of the MWCNTs appeared to increase after coating with mesoporous silica (Figure S3). Similar morphologies were observed in the MWCNT-Ag and MWCNT-AST formulations (Figure 2). These results confirm that the method of coating MWCNTs with mesoporous silica and loading AgNPs via TSD condensation reaction does not damage the surface or shape morphology of the MWCNTs.

Zeta Potential, Particles Size, and PDI

DLS and ELS analyses were performed to determine the particle size, dispersion, and stability of the MWCNT formulations. The MWCNT formulations had a size of approximately 1000~1500 nm (Figure 3). The PDI of MWCNTs was 0.75 ± 0.02, and that of MWCNT-Silica was 0.48 ± 0.06. The PDI is measured as a value between 0 and 1, and a lower value indicates a higher dispersibility.[87] Pure MWCNTs have strong aggregation and thus are difficult to use as a carrier due to their low dispersibility.[88] These results suggest that coating MWCNTs with mesoporous silica can improve their dispersibility. The combination with TSD did not significantly affect the dispersion of MWCNT-Silica, and the PDI of MWCNT-AST 10 was 0.36 ± 0.02. The Zeta potential values of MWCNTs were −24.69 ± 2.46 and MWCNT-Silica were −37.77 ± 1.23. The higher the absolute zeta value, the higher the safety of the colloid.[89] This confirmed that the mesoporous silica coating improved the stability of MWCNTs. After binding with TSD, the charge changed from negative to positive. In the MWCNT-AST formulations, the zeta potential tended to decrease as the concentration of AST extract increased. This is suggested to be because of AST with a negative charge.

FT-IR

The functional group changes of AST and MWCNT formulations were analyzed through FT-IR (Figure 4). The 934 cm^{-1} peak of MWCNT-Silica disappeared after TSD synthesis. The frequency band at 934 cm^{-1} is attributed to the stretching

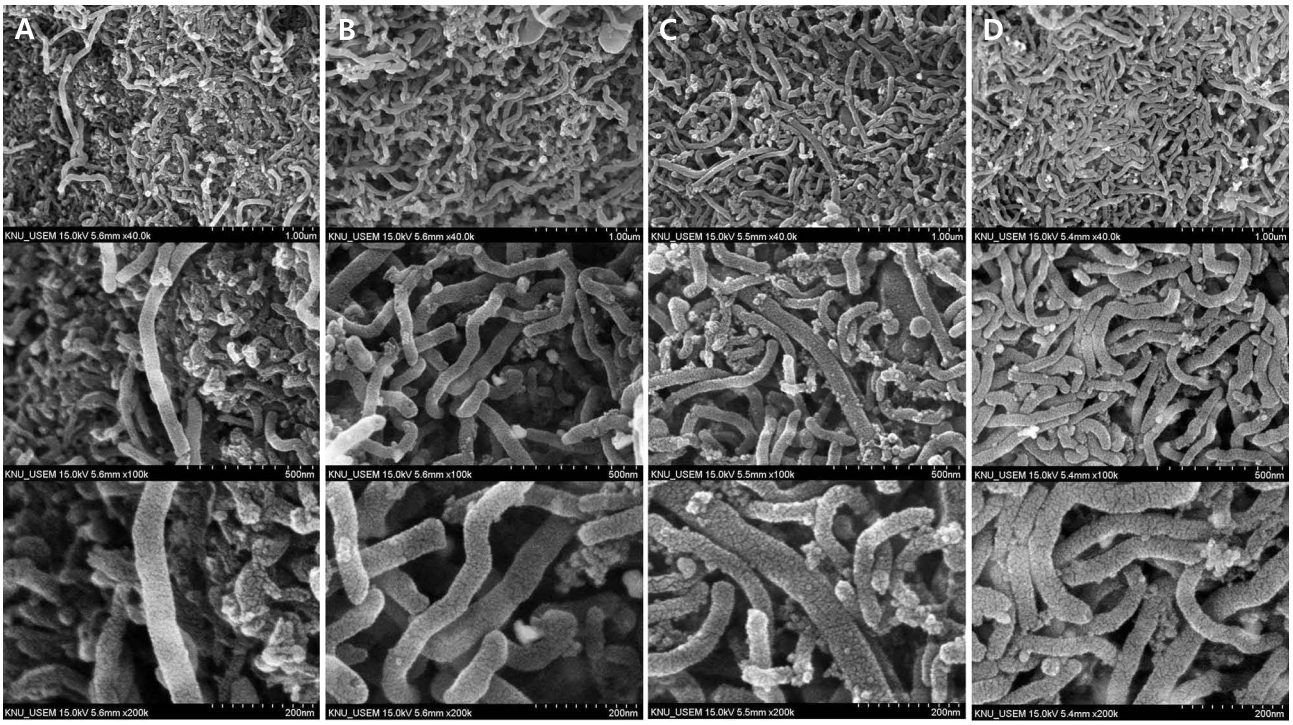

Figure 2 SEM image of various MWCNT formulations. (**A**) MWCNT-Ag; (**B**) MWCNT-AST 1; (**C**) MWCNT-AST 5; (**D**) MWCNT-AST 10.

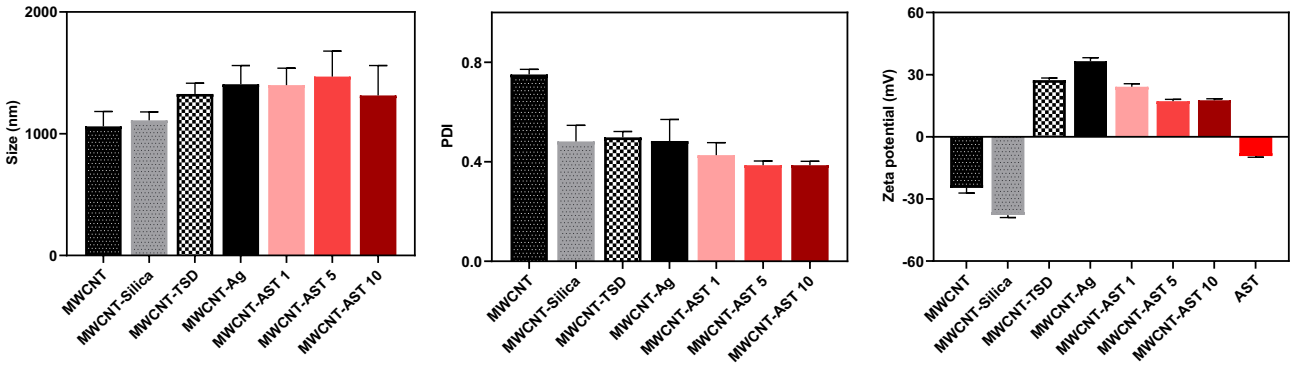

Figure 3 Particle size, PDI, and Zeta potentials of various MWCNT formulations and AST.

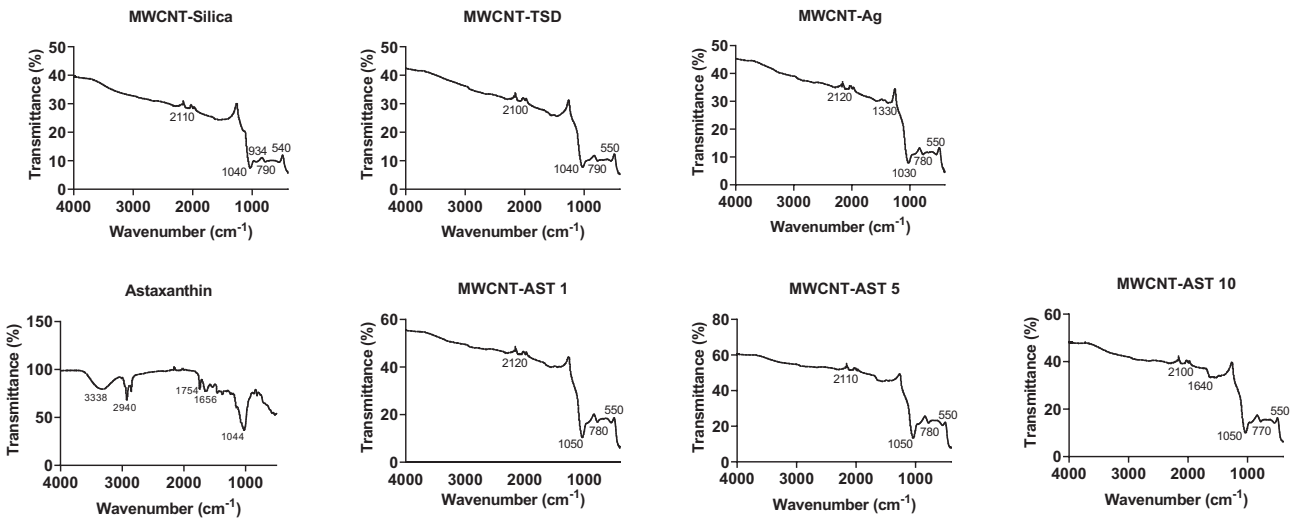

Figure 4 The FT-IR spectra of AST and MWCNT formulations.

vibration of Si-OH or SiO- groups.[90] This shows that TSD was bound to the silanol group of MWCNT-Silica. The peak near 1330 cm^{-1} may appear in the presence of a nitro group due to NO_2 asymmetric stretching vibration.[91] We suggest that the disappearance of this peak from MWCNT-AST is caused by the AST extract reducing the silver ions of MWCNT-Ag. For MWCNT-AST 10, the peak at 1656 cm^{-1} of AST shifted slightly to the peak at 1640 cm^{-1}. This represents the amide I vibration band.[92] The change in position of the amide I vibration band is mainly associated with the C=O (carbonyl) stretching vibration.[93] AST can bind to metal ions and change the electron density of the C=O bond. This causes the peak to shift to lower frequencies. In MWCNT-AST 1 and MWCNT-AST 5, peaks overlapping with AST could not be identified. In the case of MWCNT-AST formulations, the amount of AST AgNPs contained in MWCNT-Silica is very small. Therefore, it may be difficult to identify the FT-IR peak of AST in MWCNT-AST formulations. In the case of MWCNT-AST 10, it is estimated that the peak appears at 1640 cm^{-1} due to AST AgNPs attached to the MWCNT-Silica surface, as confirmed in the TEM results.

X-Ray Diffraction (XRD)

The structural properties of the MWCNT formulations were studied via XRD at 2 theta angles (Figure 5). In the case of MWCNT-Silica and MWCNT-TSD, (#002) and (#100) peaks, which are characteristic peaks of Carbon, were confirmed.[94] The XRD patterns of MWCNT-Ag and MWCNT-AST formulations showed peaks at approximately 38°, 64°, and 77°, corresponding to the (111), (220), and (311) planes of Bragg's reflections, respectively. This confirms the existence of AgNPs with a face-centered cubic structure.[95] The XRD pattern confirmed that MWCNT-Silica and AST

https://doi.org/10.2147/IJN.S485722

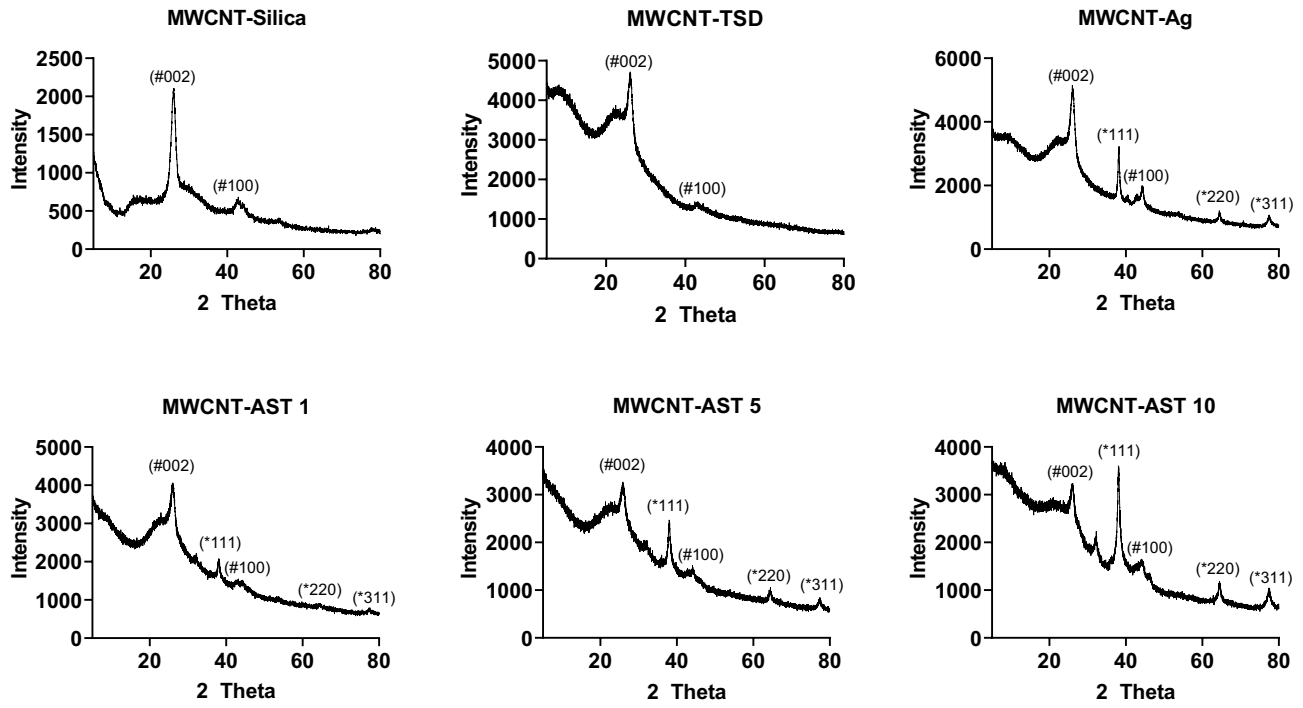

Figure 5 The XRD pattern; #: Carbon; *: Ag.

AgNPs were combined. In the case of MWCNT-AST 1, the peaks of (*220) and (*311) were weak, and it was confirmed that the peaks became stronger and clearer as the concentration of the extract increased. This could be attributed to the higher concentration of AST extract incorporated during the synthesis of MWCNT-AST formulations, as observed in the TEM results, resulting in larger-sized AgNPs formation. Furthermore, the XRD analysis of MWCNT-AST formulations is aimed at assessing the crystallinity of both MWCNTs and AgNPs incorporated into MWCNTs. Consequently, the crystallinity of AgNPs in MWCNT-AST 1 formulation, which is presumed to contain relatively smaller particles, may not be as clearly discernible.

Raman spectroscopy

Raman spectroscopy analysis showed the G band (graphene crystallinity) showing the crystallinity of CNTs and the D band showing defects (Figure 6). The G band appears in carbon nanostructures made of sp^2 bonds and can be used to determine whether MWCNTs have an ordered structure or many defects.[96] Since the D band appears strongly when there are defects or amorphous components in the carbon structure, the degree of defects in the nanotubes can be evaluated through the ratio of the D band and G band (D/G). The D+G band is located around ~2900 cm^{-1}, and the intensity of the band increases with the higher defect density. The G' band is the second harmonic of the G band, which occurs independently of the D band and mainly occurs in sp^2 carbon structures with high crystallinity. There was no significant difference in the ratio of the D band and G band in MWCNTs, MWCNT-Silica, MWCNT-TSD, and MWCNT-Ag. It was confirmed that the D band ratio increased in MWCNT-AST 5 and MWCNT-AST 10. During the process of loading AgNPs onto MWCNTs, chemical changes may occur on the surface of the CNTs, and when oxygen or silver ions bind to the carbon structure, defects or deformations occur, increasing the D band. Defects in MWCNTs affect the electron cloud, creating an environment in which reactive substances such as reactive oxygen species (ROS) are easily generated.[97] This is one of the main mechanisms for enhancing antibacterial properties. Reactive oxygen species destroy bacterial cell membranes and damage internal proteins and DNA, inhibiting bacterial survival.[98] Nanotube surfaces with many defects exhibit higher reactivity when in contact with bacterial cells, and the effect of damaging cell membranes through physical contact increases. When combined with silver nanoparticles, additional antibacterial effects can be added as silver is released. AST and AgNPs have antioxidant, antibacterial, and anticancer properties, respectively, so they can perform

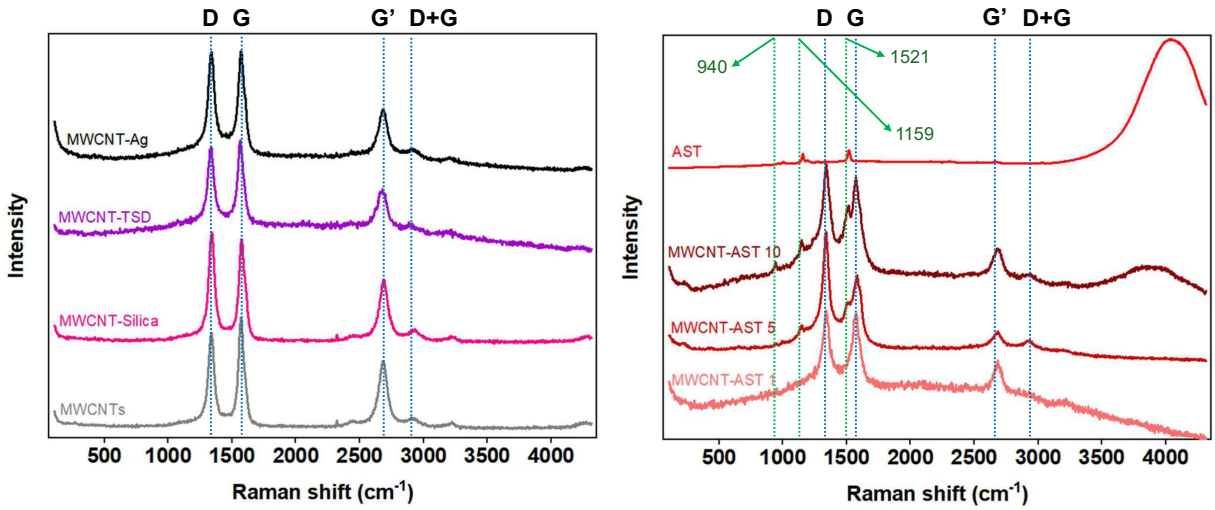

Figure 6 The Raman spectroscopy of MWCNT formulations and AST.

these functions more effectively when the defects of MWCNTs increase. In summary, as the defects of MWCNTs increase due to the increase in D bands, they are more likely to contribute to antibacterial and anticancer activities, which can have a positive effect on enhancing antibacterial and anticancer properties. The MWCNT-AST formulations showed that as the concentration of AST extract increased, the peaks corresponding to the Raman peaks of AST at 940, 1159, and 1521 cm^{-1} increased.[99,100]

TGA

TGA can analyze the composition of a mixture by independently determining the thermal properties of each component when the mixed material decomposes at different temperatures.[101] The thermal properties of AST and MWCNT formulations were analyzed in the range of 30 to 1000 °C at a heating rate of 10 °C min^{-1} and N_2 atmosphere. MWCNTs showed almost no weight loss up to 1000 °C (Figure 7). MWCNT-Silica showed slightly higher weight loss than MWCNTs, and MWCNT-TSD showed more weight loss. This can be attributed to the removal of water molecules and thermal decomposition during the Si-OH condensation reaction occurring on the silica surface.[102] The MWCNT-AST formulations showed higher thermal weight loss than MWCNT-Ag. This is thought to be because AST is used as a reducing agent for silver ions. AST showed a very large thermal weight loss in TGA (Figure S4). MWCNT-AST 5 and

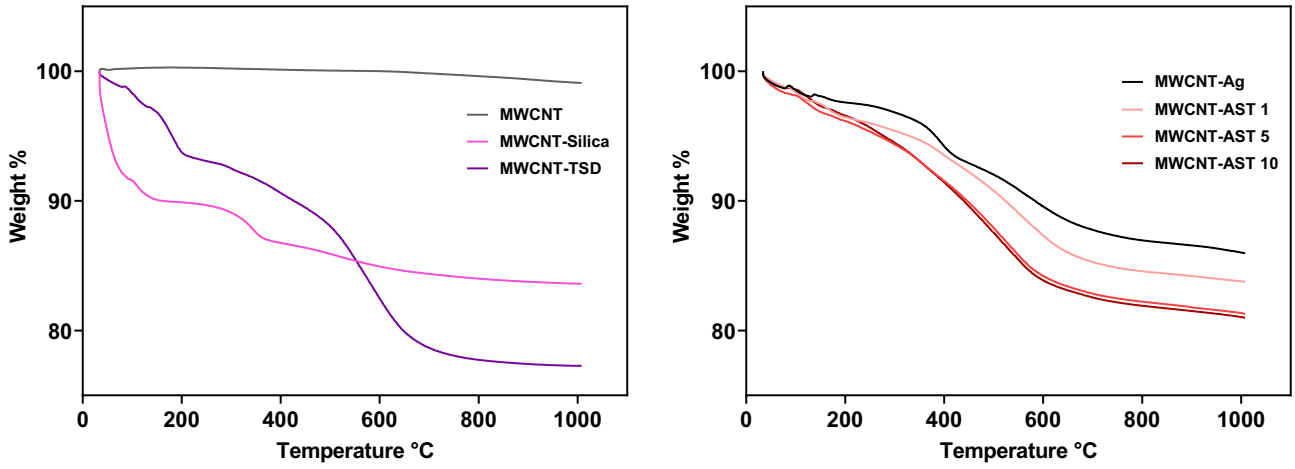

Figure 7 The TGA curve of MWCNT formulations and AST.

https://doi.org/10.2147/IJN.S485722

MWCNT-AST 10, which were found to be more bound to AST in FT-IR and Raman analyses, showed larger thermal weight losses.

Total Phenol Contents (TPC), Total Flavonoid Contents (TFC), and Antioxidant Activity

As a result of TPC and TFC analysis, almost no phenols and flavonoids were detected in MWCNT-Ag without the addition of AST extract (Figure 8A and B). MWCNT-AST 1, significantly more flavonoids were detected compared to MWCNT-Ag, but the amount of phenol detected was not significant. In MWCNT-AST 5 and MWCNT-AST 10, more amounts of phenols and flavonoids were detected compared to MWCNT-AST 1 due to the increase in AST extract concentration. In the ABTS radical scavenging activity assay and the DPPH radical scavenging activity assay, the IC_{50} values of MWCNT-Ag were 836.5 and 351.78 μg/mL, showing very low antioxidant activity (Figure 8C and D). The IC_{50} values of MWCNT-AST 1, MWCNT-AST 5, and MWCNT-AST 10 were each 393.75, 155.17, and 144.18 μg/mL in the ABTS radical scavenging activity assay. MWCNT-AST 5 and MWCNT-AST 10 showed higher antioxidant activity compared to MWCNT-AST 1. In the DPPH radical scavenging activity analysis, MWCNT-AST 5 and MWCNT-AST 10 showed high antioxidant activity. However, MWCNT-AST 1 showed a similar level of antioxidant activity as MWCNT-Ag.

Biofilm Inhibition and Destruction Test

The biofilm inhibition and destruction activities of MWCNT formulations were investigated against *E. coli, S. aureus*, and MRSA (Figure 9). MWCNT-AST showed higher biofilm inhibition and destruction activity than MWCNT-Ag in all

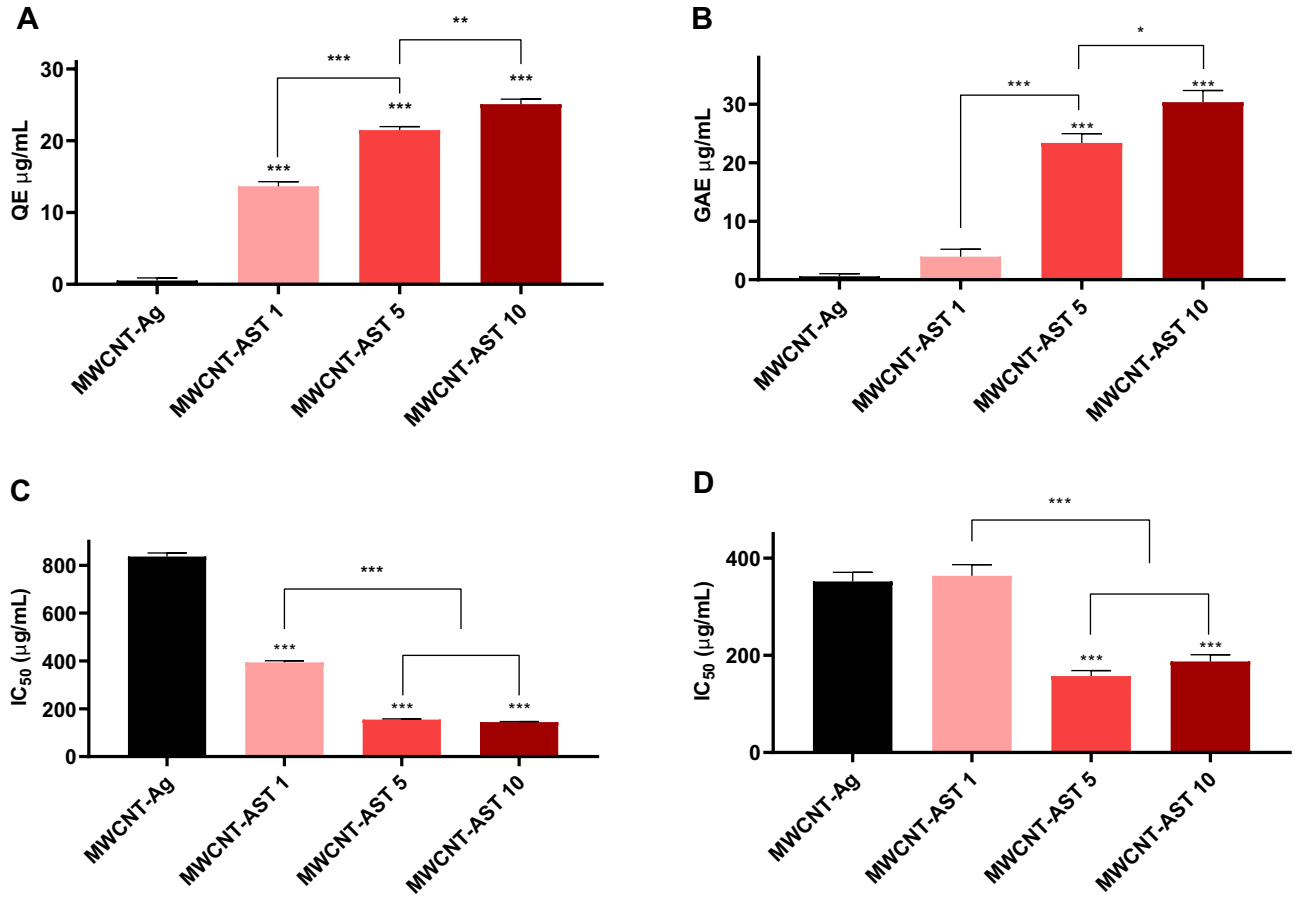

Figure 8 (**A**) TFC, (**B**) TPC, IC_{50} value of (**C**) ABTS, and (**D**) DPPH results of MWCNT formulations. Data are expressed as means ± standard deviation (n = 3). *P < 0.1, **P < 0.01, *** p < 0.001.

 https://doi.org/10.2147/IJN.S485722

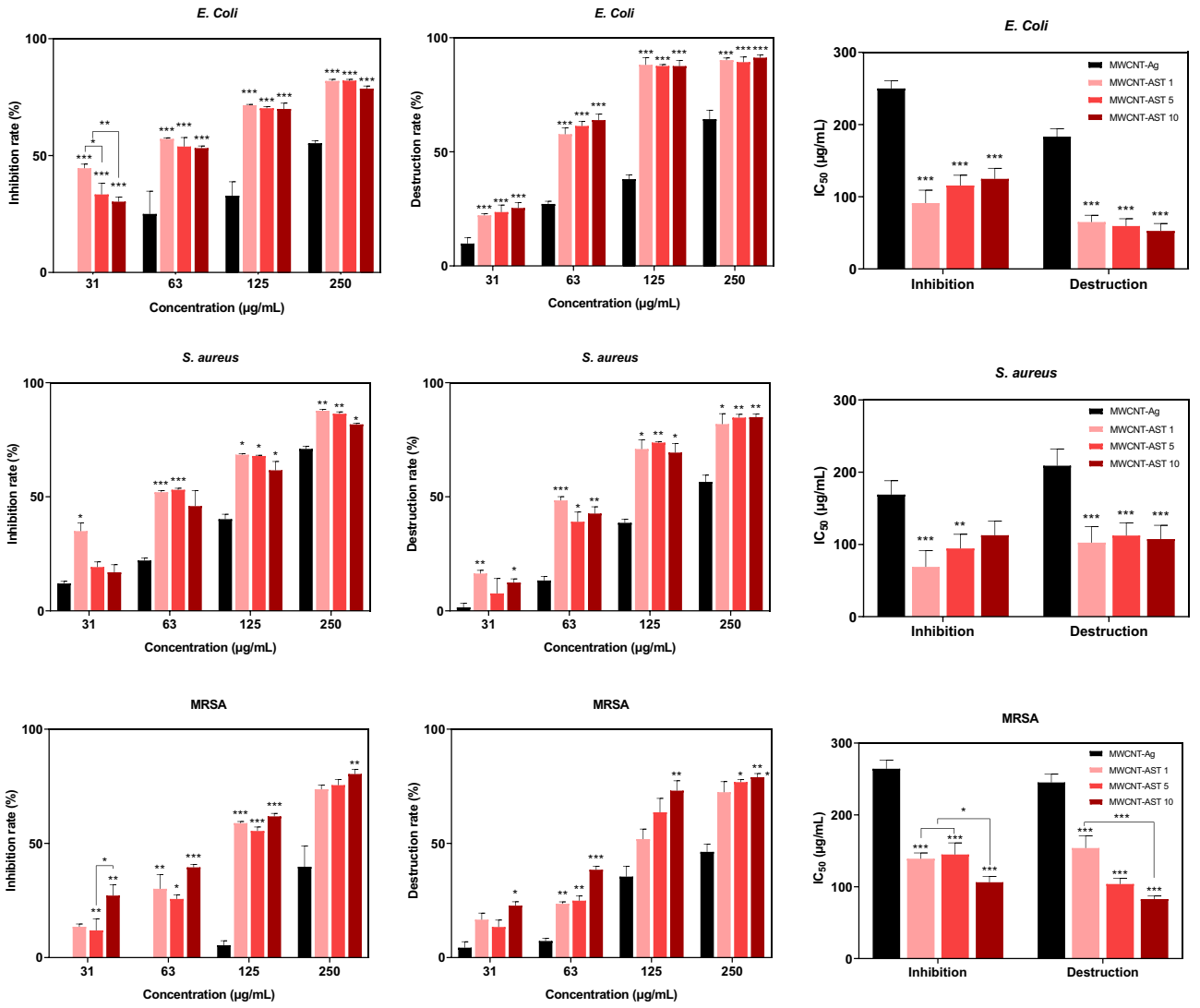

Figure 9 Biofilm inhibition and destruction activities of MWCNT formulations. Data are expressed as means ± standard deviation (n = 3). *P < 0.1, **P < 0.01, ***p < 0.001.

bacteria. In *E. coli*, MWCNT-Ag did not show biofilm inhibition activity at 31 μg/mL. MWCNT-AST 1, 5, and 10 showed high biofilm inhibition activity against *E. coli* at 44.61, 33.36, and 30.28%, respectively. The biofilm destruction result showed a similar trend. MWCNT-Ag showed the lowest biofilm inhibition and destruction activity at all concentrations against *S. aureus*. In MRSA, MWCNT-Ag did not show biofilm inhibitory activity until 63 μg/mL. MWCNT-AST 1, 5, and 10 showed high biofilm inhibitory activity at 13.47, 11.93, and 27.16%, respectively at a concentration of 31 μg/mL. In MRSA, MWCNT-AST 10 showed the lowest IC_{50} value for inhibition and destruction activity.

SEM of MRSA

SEM analysis was performed to visually confirm the antibiofilm activity of the MWCNT formulations against MRSA bacteria. The control was treated with PBS and exhibited a smooth spherical morphology (Figure 10). MRSA treated with MWCNT-Ag exhibited a morphology like the control. On the other hand, the cell membranes of MRSA treated with MWCNT-AST formulations were found to be broken or very bumpy in shape. In addition, most of the bacteria were surrounded by MWCNT-AST. This is related to the unique antibacterial activity of MWCNTs. The antibacterial mechanism of CNTs is through penetration of microbial cell walls and induction of structural damage.[103] Short CNTs can penetrate bacterial cell walls and membranes, while long CNTs envelop bacteria and interfere with their function.[104]

https://doi.org/10.2147/IJN.S485722

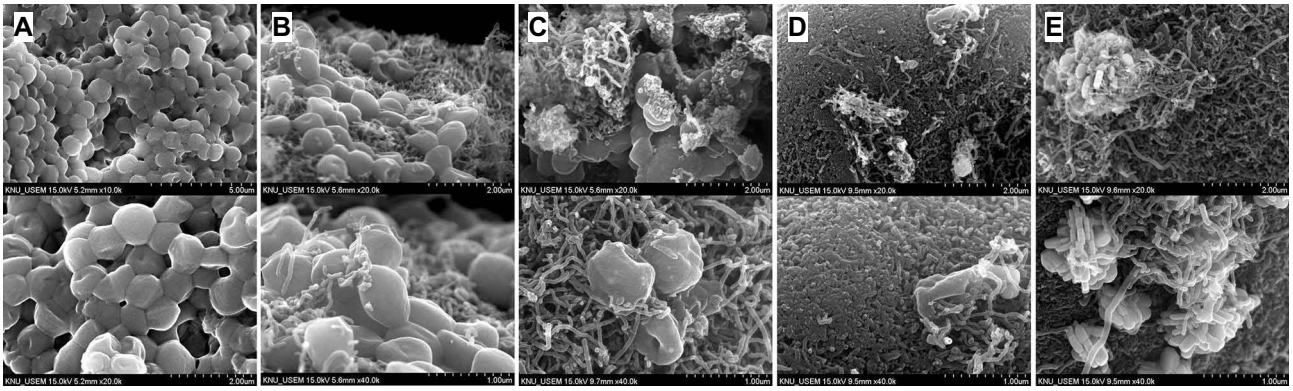

Figure 10 SEM images of MRSA treated with MWCNT formulations. (**A**) Control, (**B**) MWCNT-Ag, (**C**) MWCNT-AST 1, (**D**) MWCNT-AST 5, (**E**) MWCNT-AST 10.

CLSM

Figure 11 shows the CLSM evaluation of MRSA biofilms treated with MWCNT formulations using Calcein-AM and PI. MRSA treated with MWCNT-Ag showed slightly fewer viable cells and slightly increased dead cells compared to the control. It also showed slightly reduced biofilm thickness compared to the control. On the other hand, MRSA treated with

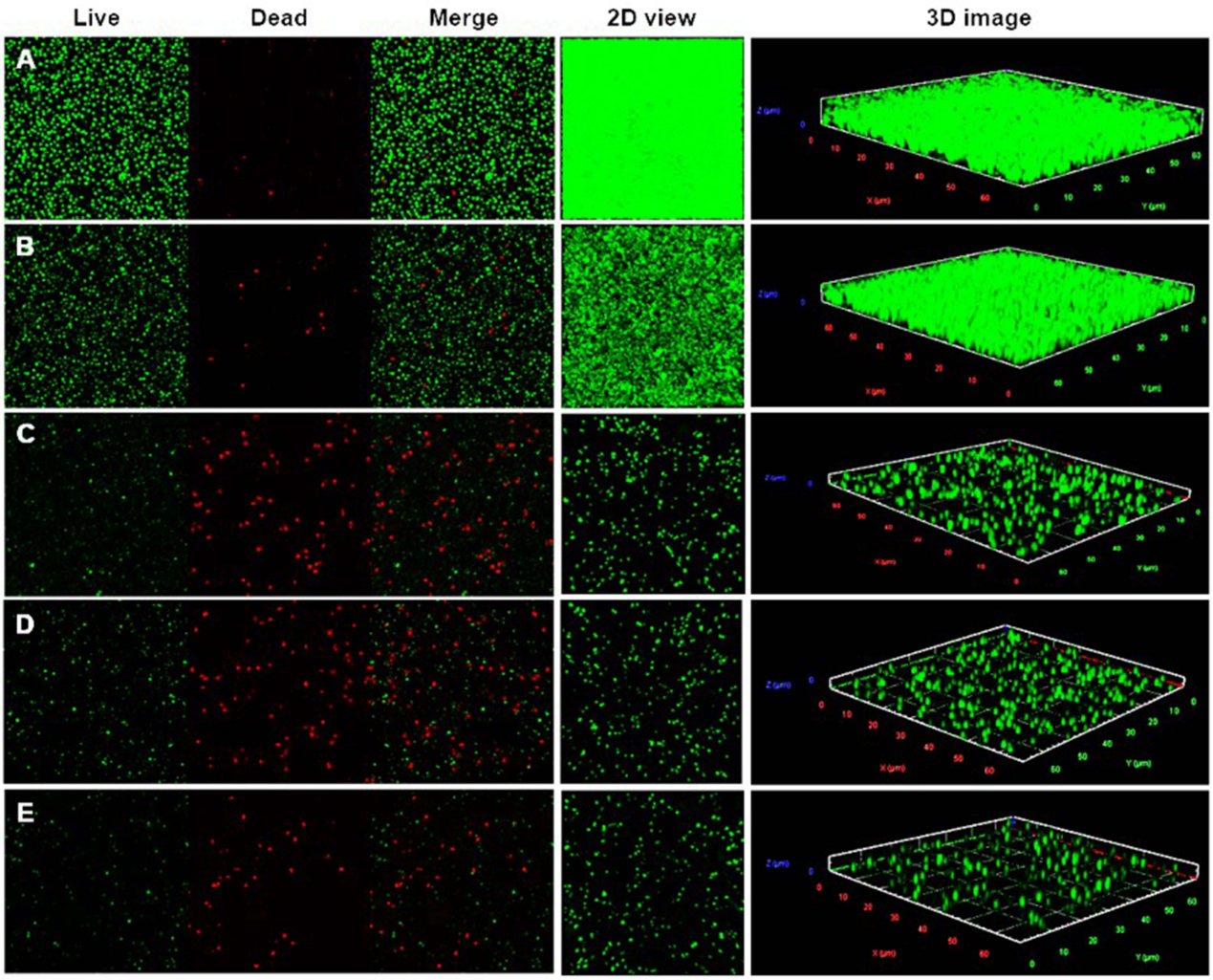

Figure 11 CLSM images of MRSA treated with (**A**) Control, (**B**) MWCNT-Ag, (**C**) MWCNT-AST 1, (**D**) MWCNT-AST 5, (**E**) MWCNT-AST 10.

MWCNT-AST formulations showed significantly reduced viable cells and significantly increased dead cells, and the biofilm thickness was also significantly thinner.

Cytotoxicity

Cytotoxicity was tested against human breast cancer cells MDA-MB-231, normal mouse skin cells NIH3T3, and normal human skin keratinocytes HaCaT. As a result of the toxicity test on NIH3T3, MWCNT-Ag showed a cell viability of 77.26% at 125 μg/mL at 24 hours, showing slight toxicity (Figure 12A). On the other hand, all MWCNT-AST formulations showed a cell viability of more than 80%, indicating that AST extract could alleviate the cytotoxicity of MWCNT-Ag. MWCNT-AST 10 showed the highest cell viability at all concentrations. To confirm the long-term toxicity of the MWCNT formulations, toxicity tests at 48 and 72 hours were also performed. At 48 hours, MWCNT-AST 1 and 5 also showed slightly increased toxicity, showing cell viability of 60.69% and 69.61% at 125 μg/mL, respectively. Even at 72 hours, MWCNT-Ag showed the highest toxicity, and MWCNT-AST 10 showed the lowest toxicity. In the toxicity test on HaCaT, no toxicity was found in all formulations up to 62 μg/mL at 24 hours (Figure 12B). MWCNT-Ag showed toxicity with a cell viability of 75.16% at a concentration of 125 μg/mL. MWCNT-AST 1 showed toxicity with a cell viability of 66.71% at a concentration of 250 μg/mL, and MWCNT-AST 5 showed a cell viability of 70.21% at a concentration of 500 μg/mL. MWCNT-AST 10 showed the lowest toxicity with a viability of 60.26% at a concentration of 1000 μg/mL. At 48 and 72 hours, MWCNT-Ag showed the highest toxicity, and MWCNT-AST 10 showed the lowest toxicity. It was confirmed that the higher the concentration of AST extract, the lower the toxicity to normal cells. In our previous study, we confirmed the toxicity of MWCNTs, MWCNT-Silica, and MWCNT-TSD to normal mouse skin cells L929. They showed toxicity at 150 μg/mL, and MWCNT-Ag showed a low survival rate even at 25 μg/mL, confirming high toxicity.[86]

As a result of the toxicity test on MDA-MB-231, MWCNT-Ag showed a survival rate of more than 80% up to 125 μg/mL, confirming low anticancer activity. MWCNT-AST 1, MWCNT-AST 5, and MWCNT-AST 10 showed survival rates of 53.60, 55.38, and 55.24% in 125 μg/mL, respectively, confirming enhanced anticancer activity. From concentrations above 250 μg/mL, low survival rates were observed in the following order: MWCNT-AST 10, MWCNT-AST 5, MWCNT-AST 1, and MWCNT-Ag. At 1000 μg/mL, the cell survival rate of MWCNT-Ag was 46.74%, and the survival rate of MWCNT-AST 10 was 15.99%, showing anticancer activity about 2.92 times higher than that of MWCNT-Ag.

Fluorescent Staining Analysis

AO/EB is a staining reagent used to analyze cell death and appears red in damaged or dead cells and green in living cells.[105] The anti-cancer activity of MWCNT-Ag and MWCNT-AST 10 was confirmed by fluorescence staining analysis (Figure 13). The results showed that MWCNT-Ag did not show significant cell death compared to the control at a concentration of 250 μg/mL, and at a concentration of 500 μg/mL, the number of living cells decreased slightly, but the morphology of the cells was not significantly damaged. MWCNT-AST 10 showed partial cell death at a concentration of 250 μg/mL and more cell death at a concentration of 500 μg/mL. The green-colored cells also showed significant morphological damage, confirming the high anticancer activity of MWNT-AST 10.

PI stains the nuclei of dead cells and does not stain living cells; dead cells appear red.[106] In the control group, few cells were stained. Stained cells were confirmed to increase in a concentration-dependent manner at 250 and 500 μg/mL of MWCNT-Ag. 250 μg/mL of MWCNT-AST 10 showed cells stained at a similar level to 500 μg/mL of MWCNT-Ag, confirming higher anticancer activity. MWCNT-AST 10 was confirmed to have a reduced number of stained cells at 500 μg/mL. This suggests that the dead cells were removed during the washing process.[107] Loss of mitochondrial membrane potential in cancer cells can induce apoptosis.[105] Rh123 indicates the loss of cell mitochondrial membrane potential. Live cells stain red, while dead cells are barely visible or appear a very dark red. The control group and 250 μg/mL of MWCNT-Ag showed similar levels of red-stained cells, and although the number decreased at 500 μg/mL, they showed lower anticancer activity than 250 μg/mL of MWCNT-AST 10. At 500 μg/mL of MWCNT-AST 10, red-stained cells were barely visible.

https://doi.org/10.2147/IJN.S485722

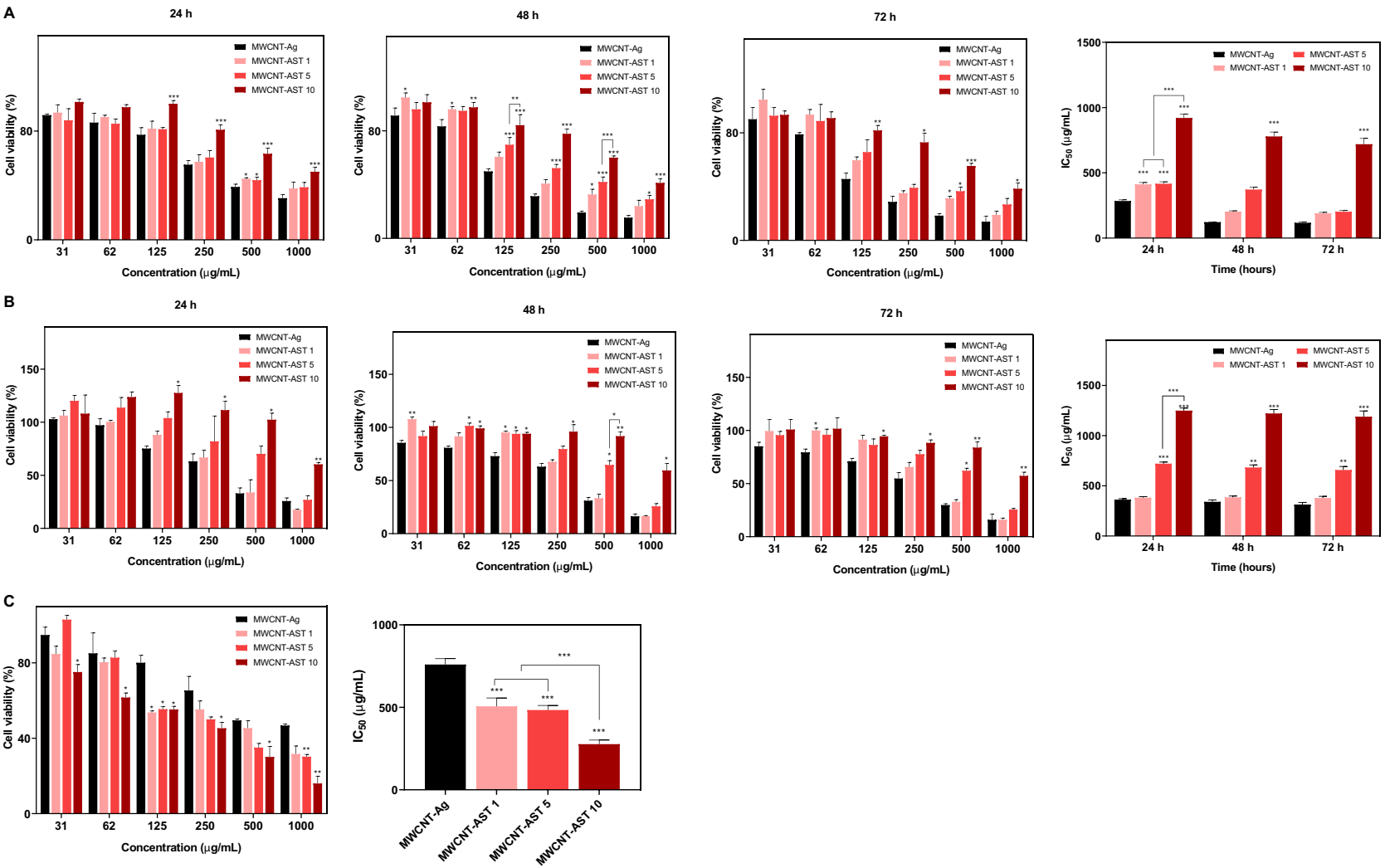

Figure 12 Cytotoxicity of MWCNT formulations in normal mouse skin cells NIH3T3 (**A**), normal human skin cells HaCaT (**B**), and breast cancer cells MDA-MB-231 (**C**). Data are expressed as means ± standard deviation (n = 3). *P < 0.1, **P < 0.01, ***P < 0.001.

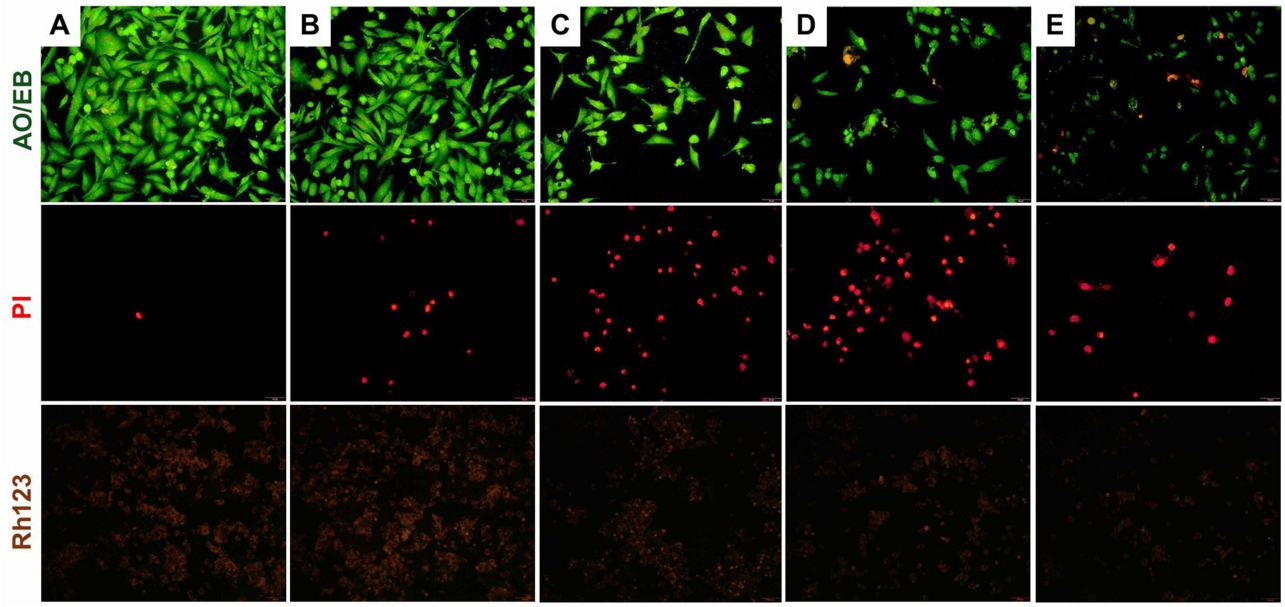

Figure 13 Fluorescence staining analysis of MDA-MB-231 cells treated with (**A**) Control, (**B**) MWCNT-Ag 250 μg/mL, (**C**) MWCNT-Ag 500 μg/mL, (**D**) MWCNT-AST 10 250 μg/mL, (**E**) MWCNT-AST 10 500 μg/mL. All experiments were performed in triplicate.

Flow Cytometry Analysis

Cells undergoing apoptosis cause abnormalities in the cell plasma membrane, such as membrane asymmetry and changes in permeability. Phosphatidyl serine (PS) exists inside the cell in healthy cells, but when the cell enters the apoptosis stage, the PS present inside the cell is exposed to the outside due to membrane changes.[108] Annexin V binds to externally exposed PS and at the same time stains dead cells with PI, allowing the degree and stage of cell death to be confirmed. As a result of the experiment, it was confirmed that cell death did not occur in cells treated with PBS (Figure 14). MWCNT-Ag was confirmed to have 71.4% live cells, 7.2% early apoptotic cells, 16.9% apoptotic cells, and 4.5% necrotic cells. MWCNT-AST 10 was confirmed to have 47.8% live cells, 5.5% early apoptotic cells, 38.9% apoptotic cells, and 7.7% necrotic cells. MWCNT-AST 10 showed high anticancer activity with a rate of apoptotic cells more than twice that of MWCNT-Ag. The proportion of apoptotic cells in MWCNT-AST 10 was more than twice that of MWCNT-Ag, suggesting enhanced anticancer activity of MWCNT-AST 10.

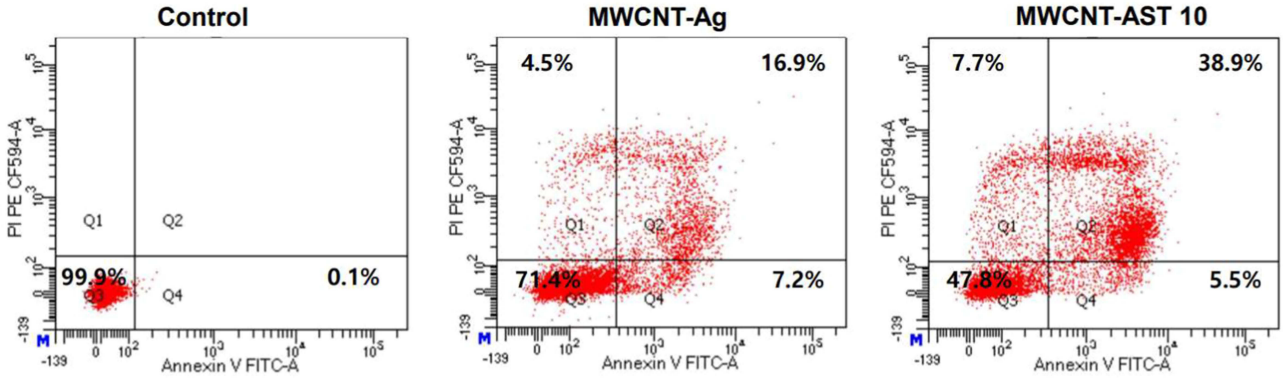

Figure 14 Apoptosis assay for MWCNT-Ag and MWCNT-AST 10 in MDA-MB-231 cells. The concentration of the sample was treated as 250 μg/mL. Control was treated with PBS.

https://doi.org/10.2147/IJN.S485722

Discussion

In this study, MWCNTs were used as carriers for AgNPs to prevent strong aggregation caused by their high surface area. Additionally, mesoporous silica was coated onto the MWCNTs to enhance their aqueous dispersibility. To enhance the antioxidant, antibiofilm, and anticancer activities of AgNPs, AST extract extracted through HME processing of *H. pluvialis* was used as a reducing solution for Ag. HPLC analysis, along with TPC and TFC results, demonstrated that HME processing increased the extraction yield of astaxanthin from *H. pluvialis* as well as the phenol and flavonoid content. This process confirmed that HPMC contributed to enhancing the water solubility of astaxanthin in *H. pluvialis* and improving the availability of active ingredients. The morphological characteristics of the prepared MWCNT formulations were examined using TEM and SEM analyses, while the distribution and quantity of AgNPs loaded onto the MWCNTs were determined through EDS analysis. TEM and EDS analyses revealed that MWCNT-AST exhibited more uniform and abundant AgNPs compared to MWCNT-Ag, confirming that the AST extract enhanced the reduction of silver ions in MWCNT-Ag. SEM analysis further confirmed that the mesoporous silica coating and AgNP loading did not cause any damage or deformation to the shape and surface of the MWCNTs. Additionally, the PDI index of MWCNT-Silica, which was lower than that of MWCNTs, indicated that the mesoporous silica coating improved the aqueous dispersibility of the MWCNTs. The zeta potential value of MWCNT-Silica also increased compared to MWCNTs, suggesting enhanced colloidal stability due to the mesoporous silica coating. In the analysis of phenol and flavonoid content, MWCNT-Ag showed barely detectable levels, but MWCNT-AST formulations showed increased phenol and flavonoid content as the concentration of added AST extract increased. In the antioxidant experiment, WMCNT-Ag showed very low antioxidant activity, while MWCNT-AST 5 and MWCNT-AST 10 showed significantly increased antioxidant activity. This is suggested to be an effect of AST, which has much higher antioxidant activity than vitamin E. Phenols and flavonoids may be involved in antioxidant activity.[109,110] It is suggested that the low antioxidant activity of MWCNT-AST 1 is due to its low phenolic and flavonoid content. *E. coli* is a facultative anaerobic bacterium found in the gastrointestinal tract of humans and animals, capable of causing a range of diseases in both.[111] *S. aureus* is a Gram-positive spherical bacterium with diverse virulence factors.[112] It is a leading cause of heart, lung, bone-joint, skin, and soft tissue infections and can lead to foodborne toxin infections.[113] MRSA is one of the major proliferating resistant bacterial pathogens causing bloodstream infections (BSIs) and ventilator-associated pneumonia.[114–117] Methicillin resistance in *S. aureus* is caused by the acquisition of the mecA gene, located within a mobile element known as the staphylococcal cassette chromosome mec (SCC mec).[118] Crystal violet staining analysis against *E. coli*, *S. aureus*, and MRSA, along with SEM and CLSM analyses of MRSA, revealed low antibiofilm activity for MWCNT-Ag. In contrast, enhanced antibiofilm activity was observed in MWCNT-AST formulations. The enhanced antibiofilm activity of MWCNT-AST compared to MWCNT-Ag is attributed to the effects of the AST extract. Previous studies have reported the antibacterial activity and inhibitory activity of bacterial biofilm formation of AST extracted from *H. pluvialis*.[119,120] Secondary metabolites, such as phenol produced by living organisms including plants and microorganisms are natural antibacterial agents.[121] The increased antibacterial activity of MWCNT-AST compared to MWCNT-Ag may be attributed to the higher phenol and flavonoid contents. Additionally, as confirmed in TEM analysis, it is suggested that MWCNT-AST formulations that form more uniform and large amounts of AgNPs can release more silver ions and exhibit higher antibacterial activity.

While MWCNT-Ag showed high cytotoxicity in normal cells NIH3T3 and HaCaT, the toxicity of MWCNT-AST formulations was confirmed to be alleviated as the concentration of the added AST extract increased. Previous studies have reported the nontoxic and cytoprotective effects of AST.[122–125] AST can protect membrane components, such as phospholipids from oxidative damage by anchoring across the lipid bilayer of biological membranes.[126] It is suggested that the AST extract mitigated the totoxicity of MWCNT-Ag toward normal cells. In a toxicity test on breast cancer cells (MDA-MB-231), MWCNT-Ag exhibited high cell viability, while MWCNT-AST formulations demonstrated significantly reduced cell viability, confirming enhanced anticancer activity. As the concentration of AST extract increased, the cell viability decreased. The IC_{50} value of MWCNT-AST 10 in MDA-MB-231 cytoxicity test was 277.05 μg/mL, showing anticancer activity that was approximately 2.7 times higher than that of MWCNT-Ag (759.79 μg/mL). Cell apoptosis analysis showed that the anticancer activity of MWCNT-AST 10 was approximately twice that of MWCNT-

Ag. Cancer can be caused by the accumulation of reactive oxygen species (ROS) and oxidative stress. Excessive ROS can cause DNA damage, tumor metastasis, and tumor drug resistance, which are involved in the occurrence and development of malignant cancer tumors.[127] Astaxanthin can inhibit ROS production and reduce oxidative stress, which are involved in anticancer activity. [128,129] AST has anticancer activity against cancer cells through inducing apoptosis and inhibiting proliferation.[130] This suggests that AST extract can improve the anticancer activity of MWCNT-Ag. Personalized therapeutics based on nanomaterials are the core of next-generation medicine and have high potential in the treatment of complex diseases such as cancer. The MWCNT-AST developed in this study has antioxidant, anticancer, and antibacterial activities, suggesting the possibility of developing personalized therapeutics based on this. It is important to target only specific cancer cells in cancer treatment to minimize damage to normal cells. MWCNT-AST demonstrates the potential to efficiently target cells by leveraging the synergistic effect of mesoporous silica, MWCNTs, AST, and AgNPs. To realize this, surface modification technology capable of binding to specific ligands of cancer cells and research on targeting mechanisms is required. MWCNTs are difficult to decompose in vivo and thus may accumulate in organs. This may cause chronic inflammation, cell damage, or tissue toxicity. Although AgNPs have high antibacterial effects, they can also induce oxidative stress or inhibit mitochondrial function in normal cells. In the long term, there is a possibility that immune system overreaction or normal cell damage may occur. Therefore, long-term studies are needed to track the in vivo residence time, release route, and accumulation of MWCNT and AgNPs complexes.

Conclusion

In this study, mesoporous silica-coated MWCNTs were used as a carrier for silver nanoparticles. To enhance the antioxidant, antibiofilm, and anticancer activities of silver nanoparticles, H. *pluvialis* was treated with HME to increase AST content, and this extract was used as a reducing solution for silver ions. MWCNT-AST was confirmed to have increased phenol and flavonoid content as the concentration of AST extract increased and showed significantly improved antioxidant activity than MWCNT-Ag. MWCNT-AST showed high antibiofilm activity against *E. coli, S. aureus*, and MRSA, confirming its antibacterial activity against Gram-negative and Gram-positive bacteria, suggesting its potential as a treatment for multidrug-resistant bacteria. In the toxicity test on normal cells HacaT, MWCNT-Ag showed very high toxicity, but in MWCNT-AST formulations, it was confirmed that the cytotoxicity was alleviated as the concentration of the added AST extract increased. In MDA-MB-231 breast cancer cells, MWCNT-AST showed improved anticancer activity than MWCNT-Ag, confirming the potential of MWCNT-AST as an anticancer agent.

Abbreviations

MWCNTs, multi-walled carbon nanotubes; MWCNT-Silica, Mesoporous silica-coated MWCNTs; MWCNT-Ag, AgNPs-loaded MWCNT-Silica; MWCNT-AST, multi-walled carbon nanotubes fabricated with hot-melt extruded astaxanthin mediated synthesized silver nanoparticles; HME, hot melt extrusion; H. *pluvialis, Haematococcus pluvialis*; AST, Astaxanthin; TEM, transmission electron microscopy; SEM, Scanning electron microscopy; PDI, Polydispersity index; PI, propidium iodide; AO/EB, acridine orange/ethyl bromide; RH123, rhodamine 123; XRD, X-ray diffractometer; FT-IR, Fourier-Transform Infrared Spectroscopy; HPLC, High-performance liquid chromatography; TGA, Thermogravimetric Analysis; MIC, minimum inhibition concentration; MBC, minimum bactericidal concentration; TPC, total phenol contents; TFC, total flavonoid contents.

Research Ethics Statement

This study did not involve experiments on humans or animals.

Credit Author Statement

Han-Sol You: Conceptualization, Investigation, Methodology, Writing - original draft, Writing - review and editing. Young-Sun Jang: Methodology, Writing - review and editing, Resources, Supervision. Anbazhagan Sathiyaseelan: Project administration, Methodology, Writing - review and editing, Supervision. Su-Ji Ryu: Conceptualization, Methodology, Writing - review and editing. Ha-Yeon Lee: Investigation, Data curation. Jong-Suep Baek: Writing-

review and editing, Supervision, Funding acquisition. All authors made a significant contribution to the work reported, whether that is in the conception, study design, execution, acquisition of data, analysis and interpretation, or in all these areas; took part in drafting, revising or critically reviewing the article; gave final approval of the version to be published; have agreed on the journal to which the article has been submitted; and agree to be accountable for all aspects of the work.

Funding

This research was supported by the Korea Institute of Marine Science & Technology Promotion (KIMST) funded by the Ministry of Oceans and Fisheries (RS-2023-00254674).

Disclosure

The authors declare that they have no known competing financial interests or personal relationships that could have appeared to influence the work reported in this paper.

References

1. Alateyah N, Ahmad SM, Gupta I, et al. Haematococcus pluvialis microalgae extract inhibits proliferation, invasion, and induces apoptosis in breast cancer cells. *Front Nutr*. 2022;9:882956. doi:10.3389/fnut.2022.882956
2. Palozza P, Torelli C, Boninsegna A, et al. Growth-inhibitory effects of the astaxanthin-rich alga Haematococcus pluvialis in human colon cancer cells. *Cancer Lett*. 2009;283(1):108–117. doi:10.1016/j.canlet.2009.03.031
3. Gouveia L, Raymundo A, Batista AP, Sousa I, Empis J. Chlorella vulgaris and Haematococcus pluvialis biomass as colouring and antioxidant in food emulsions. *Eur Food Res Technol*. 2006;222(3):362–367. doi:10.1007/s00217-005-0105-z
4. Shanab SMM, Mostafa SSM, Shalaby EA, Mahmoud GI. Aqueous extracts of microalgae exhibit antioxidant and anticancer activities. *Asian Pac J Trop Biomed*. 2012;2(8):608–615. doi:10.1016/S2221-1691(12)60106-3
5. Shah MMR, Liang Y, Cheng JJ, Daroch M. Astaxanthin-producing green microalga Haematococcus pluvialis: from single cell to high value commercial products. *Front Plant Sci*. 2016;7:531. doi:10.3389/fpls.2016.00531
6. Ambati RR, Phang S-M, Ravi S, Aswathanarayana RG. Astaxanthin: sources, extraction, stability, biological activities and its commercial applications—a review. *Mar Drugs*. 2014;12(1):128–152. doi:10.3390/md12010128
7. Nakagawa K, Kiko T, Miyazawa T, et al. Antioxidant effect of astaxanthin on phospholipid peroxidation in human erythrocytes. *Br J Nutr*. 2011;105(11):1563–1571. doi:10.1017/S0007114510005398
8. Merhan O. The biochemistry and antioxidant properties of carotenoids. *Carotenoids*. 2017;5:51.
9. Donoso A, González-Durán J, Muñoz AA, González PA, Agurto-Muñoz C. Therapeutic uses of natural astaxanthin: an evidence-based review focused on human clinical trials. *Pharmacol Res*. 2021;166:105479. doi:10.1016/j.phrs.2021.105479
10. Yuan JP, Peng J, Yin K, Wang JH. Potential health-promoting effects of astaxanthin: a high-value carotenoid mostly from microalgae. *Mol Nutr Food Res*. 2011;55(1):150–165. doi:10.1002/mnfr.201000414
11. Kim SH, Kim H. Inhibitory effect of astaxanthin on oxidative stress-induced mitochondrial dysfunction-a mini-review. *Nutrients*. 2018;10(9):1137. doi:10.3390/nu10091137
12. Koller M, Muhr A, Braunegg G. Microalgae as versatile cellular factories for valued products. *Algal Res*. 2014;6:52–63. doi:10.1016/j.algal.2014.09.002
13. Kumar S, Kumar R, Kumari A, Panwar A. Astaxanthin: a super antioxidant from microalgae and its therapeutic potential. *J Basic Microbiol*. 2022;62(9):1064–1082. doi:10.1002/jobm.202100391
14. Simões MF, Pinto RMA, Simões S. Hot-melt extrusion in the pharmaceutical industry: toward filing a new drug application. *Drug Discovery Today*. 2019;24(9):1749–1768. doi:10.1016/j.drudis.2019.05.013
15. Kim H-B, Ryu S, Baek J-S. The effect of hot-melt extrusion of mulberry leaf on the number of active compounds and antioxidant activity. *Plants*. 2022;11(22):3019. doi:10.3390/plants11223019
16. Crowley MM, Zhang F, Repka MA, et al. Pharmaceutical applications of hot-melt extrusion: part I. *Drug Dev Ind Pharm*. 2007;33(9):909–926. doi:10.1080/03639040701498759
17. Go EJ, Ryu BR, Ryu SJ, et al. An enhanced water solubility and stability of anthocyanins in mulberry processed with hot melt extrusion. *Int J Mol Sci*. 2021;22(22):12377. doi:10.3390/ijms222212377
18. Sohrabi Y, Panahi-Azar V, Barzegar A, Dolatabadi JEN, Dehghan P. Spectroscopic, thermodynamic and molecular docking studies of bovine serum albumin interaction with ascorbyl palmitate food additive. *Bioimpacts*. 2017;7(4):241. doi:10.15171/bi.2017.28
19. Mehuys E, Vervaet C, Remon JP. Hot-melt extruded ethylcellulose cylinders containing a HPMC–Gelucire® core for sustained drug delivery. *J Control Release*. 2004;94(2):273–280. doi:10.1016/j.jconrel.2003.09.018
20. Chuah AM, Jacob B, Jie Z, et al. Enhanced bioavailability and bioefficacy of an amorphous solid dispersion of curcumin. *Food Chem*. 2014;156:227–233. doi:10.1016/j.foodchem.2014.01.108
21. Wang M, Cheng H, Chen S, et al. Microalgal cell disruption via extrusion for the production of intracellular valuables. *Energy*. 2018;142:339–345. doi:10.1016/j.energy.2017.10.061
22. Patel V, Berthold D, Puranik P, Gantar M. Screening of cyanobacteria and microalgae for their ability to synthesize silver nanoparticles with antibacterial activity. *Biotechnol Rep*. 2015;5:112–119. doi:10.1016/j.btre.2014.12.001
23. Sudha S, Rajamanickam K, Rengaramanujam J. Microalgae mediated synthesis of silver nanoparticles and their antibacterial activity against pathogenic bacteria. 2013.

24. Terra ALM, Kosinski RDC, Moreira JB, Costa JAV, Morais MGD. Microalgae biosynthesis of silver nanoparticles for application in the control of agricultural pathogens. *J Environ Sci Health Part B*. 2019;54(8):709–716. doi:10.1080/03601234.2019.1631098
25. Chugh D, Viswamalya V, Das B. Green synthesis of silver nanoparticles with algae and the importance of capping agents in the process. *J Genet Eng Biotechnol*. 2021;19(1):126. doi:10.1186/s43141-021-00228-w
26. Savvidou MG, Kontari E, Kalantzi S, Mamma D. Green synthesis of silver nanoparticles using the cell-free supernatant of haematococcus pluvialis culture. *Materials*. 2024;17(1). doi:10.3390/ma17010187
27. Mukherjee A, Sarkar D, Sasmal S. A review of green synthesis of metal nanoparticles using algae. *Front Microbiol*. 2021;12:693899. doi:10.3389/fmicb.2021.693899
28. Régnier P, Bastias J, Rodriguez-Ruiz V, et al. Astaxanthin from haematococcus pluvialis prevents oxidative stress on human endothelial cells without toxicity. *Mar Drugs*. 2015;13(5):2857–2874. doi:10.3390/md13052857
29. Tanaka T, Morishita Y, Suzui M, Kojima T, Okumura A, Mori H. Chemoprevention of mouse urinary bladder carcinogenesis by the naturally occurring carotenoid astaxanthin. *Carcinogenesis*. 1994;15(1):15–19. doi:10.1093/carcin/15.1.15
30. Tanaka T, Kawamori T, Ohnishi M, et al. Suppression of azoxymethane-induced rat colon carcinogenesis by dietary administration of naturally occurring xanthophylls astaxanthin and canthaxanthin during the postinitiation phase. *Carcinogenesis*. 1995;16(12):2957–2963. doi:10.1093/carcin/16.12.2957
31. Tanaka T, Makita H, Ohnishi M, Mori H, Satoh K, Harã A. Chemoprevention of rat oral carcinogenesis by naturally occurring xanthophylls, astaxanthin and canthaxanthin. *Cancer Res*. 1995;55(18):4059–4064.
32. Shokrian Zeini M, Pakravesh SM, Jalili Kolour SM, et al. Astaxanthin as an anticancer agent against breast cancer: an in vivo and in vitro investigation. *Curr Med Chem*. 2024;31. doi:10.2174/0109298673288774240406053607
33. Barabadi H, Mojab F, Vahidi H, et al. Green synthesis, characterization, antibacterial and biofilm inhibitory activity of silver nanoparticles compared to commercial silver nanoparticles. *Inorg Chem Commun*. 2021;129:108647. doi:10.1016/j.inoche.2021.108647
34. Porter GC, Tompkins GR, Schwass DR, Li KC, Waddell JN, Meledandri CJ. Anti-biofilm activity of silver nanoparticle-containing glass ionomer cements. *Dent Mater*. 2020;36(8):1096–1107. doi:10.1016/j.dental.2020.05.001
35. Qin H, Cao H, Zhao Y, et al. In vitro and in vivo anti-biofilm effects of silver nanoparticles immobilized on titanium. *Biomaterials*. 2014;35(33):9114–9125. doi:10.1016/j.biomaterials.2014.07.040
36. Kotakadi VS, Gaddam SA, Venkata SK, Sai Gopal DVR. New generation of bactericidal silver nanoparticles against different antibiotic resistant Escherichia coli strains. *Appl Nanosci*. 2015;5(7):847–855. doi:10.1007/s13204-014-0381-7
37. Choi JS, Jung HC, Baek YJ, et al. Antibacterial activity of green-synthesized silver nanoparticles using areca catechu extract against antibiotic-resistant bacteria. *Nanomaterials*. 2021;11(1):205. doi:10.3390/nano11010205
38. Zhang L, Gu F, Chan J, Wang A, Langer R, Farokhzad O. Nanoparticles in medicine: therapeutic applications and developments. *Clin Pharmacol Ther*. 2008;83(5):761–769. doi:10.1038/sj.clpt.6100400
39. Paddle-Ledinek JE, Nasa Z, Cleland HJ. Effect of different wound dressings on cell viability and proliferation. *Plastic and Reconstructive Surgery*. 2006;117(7S):110S–118S. doi:10.1097/01.prs.0000225439.39352.ce
40. Martínez-Gutierrez F, Thi EP, Silverman JM, et al. Antibacterial activity, inflammatory response, coagulation and cytotoxicity effects of silver nanoparticles. *Nanomed Nanotechnol Biol Med*. 2012;8(3):328–336. doi:10.1016/j.nano.2011.06.014
41. Martinez-Gutierrez F, Boegli L, Agostinho A, et al. Anti-biofilm activity of silver nanoparticles against different microorganisms. *Biofouling*. 2013;29(6):651–660. doi:10.1080/08927014.2013.794225
42. De la Fuente-Núñez C, Reffuveille F, Fernández L, Hancock RE. Bacterial biofilm development as a multicellular adaptation: antibiotic resistance and new therapeutic strategies. *Curr Opin Microbiol*. 2013;16(5):580–589. doi:10.1016/j.mib.2013.06.013
43. Lebeaux D, Ghigo J-M, Beloin C. Biofilm-related infections: bridging the gap between clinical management and fundamental aspects of recalcitrance toward antibiotics. *Microbiol Mol Biol Rev*. 2014;78(3):510–543. doi:10.1128/MMBR.00013-14
44. Padmavathi AR, Bakkiyaraj D, Pandian SK. Biofilm inhibition by natural products of marine origin and their environmental applications. *Biofilms Plant Soil Health*. 2017:465–478.
45. Kannappan A, Durgadevi R, Srinivasan R, et al. 2-Hydroxy-4-methoxybenzaldehyde from Hemidesmus indicus is antagonistic to Staphylococcus epidermidis biofilm formation. *Biofouling*. 2020;36(5):549–563. doi:10.1080/08927014.2020.1777989
46. Cepas V, López Y, Muñoz E, et al. Relationship between biofilm formation and antimicrobial resistance in gram-negative bacteria. *Microb Drug Resist*. 2019;25(1):72–79. doi:10.1089/mdr.2018.0027
47. Khatoon Z, McTiernan CD, Suuronen EJ, Mah T-F, Alarcon EI. Bacterial biofilm formation on implantable devices and approaches to its treatment and prevention. *Heliyon*. 2018;4(12):e01067. doi:10.1016/j.heliyon.2018.e01067
48. Liyanage PY, Hettiarachchi SD, Zhou Y, et al. Nanoparticle-mediated targeted drug delivery for breast cancer treatment. *Biochimica et Biophysica Acta*. 2019;1871(2):419–433. doi:10.1016/j.bbcan.2019.04.006
49. Varricchio CG. *A Cancer Source Book for Nurses*. Jones & Bartlett Learning; 2004.
50. American Cancer Society. *Breast Cancer Facts & Figures*. American Cancer Society; 2007.
51. Gautam L, Jain A, Shrivastava P, Vyas S, Vyas SP. Chapter 1 - Emergence of novel targeting systems and conventional therapies for effective cancer treatment. In: Yadav AK, Gupta U, Sharma R, editors. *Nano Drug Delivery Strategies for the Treatment of Cancers*. Academic Press; 2021:1–35.
52. Garcia-Oliveira P, Otero P, Pereira AG, et al. Status and challenges of plant-anticancer compounds in cancer treatment. *Pharmaceuticals*. 2021;14(2):157. doi:10.3390/ph14020157
53. Rao PV, Nallappan D, Madhavi K, Rahman S, Jun Wei L, Gan SH. Phytochemicals and biogenic metallic nanoparticles as anticancer agents. *Oxid Med Cell Longev*. 2016;2016(1):3685671. doi:10.1155/2016/3685671
54. Venkatesan B, Subramanian V, Tumala A, Vellaichamy E. Rapid synthesis of biocompatible silver nanoparticles using aqueous extract of Rosa damascena petals and evaluation of their anticancer activity. *Asian Pac J Trop Med*. 2014;7:S294–S300.
55. Nayak D, Pradhan S, Ashe S, Rauta PR, Nayak B. Biologically synthesised silver nanoparticles from three diverse family of plant extracts and their anticancer activity against epidermoid A431 carcinoma. *J Colloid Interface Sci*. 2015;457:329–338. doi:10.1016/j.jcis.2015.07.012
56. Suman TY, Radhika Rajasree SR, Kanchana A, Elizabeth SB. Biosynthesis, characterization and cytotoxic effect of plant mediated silver nanoparticles using Morinda citrifolia root extract. *Colloids Surf B*. 2013;106:74–78. doi:10.1016/j.colsurfb.2013.01.037

57. Yeasmin S, Datta HK, Chaudhuri S, Malik D, Bandyopadhyay A. In-vitro anti-cancer activity of shape controlled silver nanoparticles (AgNPs) in various organ specific cell lines. *J Mol Liq*. 2017;242:757–766. doi:10.1016/j.molliq.2017.06.047
58. Top A, Silver ÜS. zinc, and copper exchange in a Na-clinoptilolite and resulting effect on antibacterial activity. *Appl Clay Sci*. 2004;27 (1):13–19. doi:10.1016/j.clay.2003.12.002
59. Kwakye-Awuah B, Radecka I, Kenward MA, Williams CD. Production of silver-doped analcime by isomorphous substitution technique. *J Chem Technol Biotechnol*. 2008;83(9):1255–1260. doi:10.1002/jctb.1938
60. Lee JS, Murphy WL. Functionalizing calcium phosphate biomaterials with antibacterial silver particles. *Adv Mater*. 2013;25(8):1173–1179. doi:10.1002/adma.201203370
61. Jia H, Hou W, Wei L, Xu B, Liu X. The structures and antibacterial properties of nano-SiO2 supported silver/zinc-silver materials. *Dent Mater*. 2008;24(2):244–249. doi:10.1016/j.dental.2007.04.015
62. Yang H, Liu Y, Shen Q, et al. Mesoporous silica microcapsule-supported Ag nanoparticles fabricated via nano-assembly and its antibacterial properties. 10.1039/C2JM35621J. *J Mater Chem*. 2012;22(45):24132–24138. doi:10.1039/C2JM35621J
63. Carmona D, Lalueza P, Balas F, Arruebo M, Santamaría J. Mesoporous silica loaded with peracetic acid and silver nanoparticles as a dual-effect, highly efficient bactericidal agent. *Microporous Mesoporous Mater*. 2012;161:84–90. doi:10.1016/j.micromeso.2012.05.012
64. Wang Y, Gu H. Core-shell-type magnetic mesoporous silica nanocomposites for bioimaging and therapeutic agent delivery. *Adv Mater*. 2015;27 (3):576–585. doi:10.1002/adma.201401124
65. Wu S-H, Mou C-Y, Lin H-P. Synthesis of mesoporous silica nanoparticles. 10.1039/C3CS35405A. *Chem Soc Rev*. 2013;42(9):3862–3875. doi:10.1039/C3CS35405A
66. Hong G, Diao S, Antaris AL, Dai H. Carbon nanomaterials for biological imaging and nanomedicinal therapy. *Chem Rev*. 2015;115 (19):10816–10906. doi:10.1021/acs.chemrev.5b00008
67. Anju VT, Paramanantham P, Sb SL, et al. Antimicrobial photodynamic activity of rose bengal conjugated multi walled carbon nanotubes against planktonic cells and biofilm of Escherichia coli. *Photodiagn Photodyn Ther*. 2018;24:300–310. doi:10.1016/j.pdpdt.2018.10.013
68. Natsuki J, Natsuki T. Silver nanoparticle/carbon nanotube hybrid nanocomposites: one-step green synthesis, properties, and applications. *Nanomaterials*. 2023;13(8):1297. doi:10.3390/nano13081297
69. Dinh NX, Quy NV, Huy TQ, Le A-T. Decoration of silver nanoparticles on multiwalled carbon nanotubes: antibacterial mechanism and ultrastructural analysis. *J Nanomater*. 2015;2015(1):814379. doi:10.1155/2015/814379
70. Xia T, Guo X, Lin Y, et al. Aggregation of oxidized multi-walled carbon nanotubes: interplay of nanomaterial surface O-functional groups and solution chemistry factors. *Env Pollut*. 2019;251:921–929. doi:10.1016/j.envpol.2019.05.079
71. Bai Y, Park IS, Lee SJ, et al. Aqueous dispersion of surfactant-modified multiwalled carbon nanotubes and their application as an antibacterial agent. *Carbon*. 2011;49(11):3663–3671. doi:10.1016/j.carbon.2011.05.002
72. Rastogi R, Kaushal R, Tripathi S, Sharma AL, Kaur I, Bharadwaj LM. Comparative study of carbon nanotube dispersion using surfactants. *J Colloid Interface Sci*. 2008;328(2):421–428. doi:10.1016/j.jcis.2008.09.015
73. Jiang L, Gao L, Sun J. Production of aqueous colloidal dispersions of carbon nanotubes. *J Colloid Interface Sci*. 2003;260(1):89–94. doi:10.1016/S0021-9797(02)00176-5
74. You H-S, Ryu S-J, Lee H-Y, Baek J-S. Enhanced antibacterial activity of multi-walled carbon nanotubes loaded with hot-melt extruded Mulberry leaf silver nanoparticles. *Colloids Surf A*. 2024;699:134522. doi:10.1016/j.colsurfa.2024.134522
75. Ryu S-J, You H-S, Lee H-Y, Baek J-S. Manufacture of mesoporous silica coated multi-walled carbon nanotubes containing silver nanoparticles synthesized by Angelica gigas Nakai using hot-melt extrusion for enhanced antimicrobial activities. *Colloids Surf A*. 2024;693:134023. doi:10.1016/j.colsurfa.2024.134023
76. Zhu Y, Xu J, Wang Y, et al. Silver nanoparticles-decorated and mesoporous silica coated single-walled carbon nanotubes with an enhanced antibacterial activity for killing drug-resistant bacteria. *Nano Res*. 2020;13(2):389–400. doi:10.1007/s12274-020-2621-3
77. da Silva JAG, de Resende MLV, Ribeiro IS, et al. Chemical composition, production of secondary metabolites and antioxidant activity in coffee cultivars susceptible and partially resistant to bacterial halo blight. *Plants*. 2021;10(9):1915. doi:10.3390/plants10091915
78. Chen S, Wang J, Tang K, et al. Multi-modal imaging monitored M2 macrophage targeting sono-responsive nanoparticles to combat MRSA deep infections. *Int J Nanomed*. 2022;17:4525–4546. doi:10.2147/ijn.S383237
79. Sathiyaseelan A, Saravanakumar K, Naveen KV, et al. Combination of Paraconiothyrium brasiliense fabricated titanium dioxide nanoparticle and antibiotics enhanced antibacterial and antibiofilm properties: a toxicity evaluation. *Environ Res*. 2022;212:113237. doi:10.1016/j.envres.2022.113237
80. Qiao Y, Liu X, Li B, et al. Treatment of MRSA-infected osteomyelitis using bacterial capturing, magnetically targeted composites with microwave-assisted bacterial killing. *Nat Commun*. 2020;11(1):4446. doi:10.1038/s41467-020-18268-0
81. Sathiyaseelan A, Saravanakumar K, Zhang X, Naveen KV, Wang M-H. Ampicillin-resistant bacterial pathogens targeted chitosan nano-drug delivery system (CS-AMP-P-ZnO) for combinational antibacterial treatment. *Int J Biol Macromol*. 2023;237:124129. doi:10.1016/j.ijbiomac.2023.124129
82. Rhoomi ZR, Ahmed DS, Jabir MS, Qadeer A, Ismael AB, Swelum AA. Fabrication of pure Bi2WO6 and Bi2WO6/MWCNTs nanocomposite as potential antibacterial and anticancer agents. *Sci Rep*. 2024;14(1):9545. doi:10.1038/s41598-024-58751-y
83. Saravanakumar K, Mariadoss AVA, Sathiyaseelan A, Wang M-H. Synthesis and characterization of nano-chitosan capped gold nanoparticles with multifunctional bioactive properties. *Int J Biol Macromol*. 2020;165:747–757. doi:10.1016/j.ijbiomac.2020.09.177
84. Rotta J, Ozório RÁ, Kehrwald AM, de Oliveira Barra GM, de Melo Castanho Amboni RD, Barreto PLM. Parameters of color, transparency, water solubility, wettability and surface free energy of chitosan/hydroxypropylmethylcellulose (HPMC) films plasticized with sorbitol. *Mater Sci Eng*. 2009;29(2):619–623. doi:10.1016/j.msec.2008.10.032
85. Ishikawa T, Watanabe Y, Takayama K, Endo H, Matsumoto M. Effect of hydroxypropylmethylcellulose (HPMC) on the release profiles and bioavailability of a poorly water-soluble drug from tablets prepared using macrogol and HPMC. *Int J Pharm*. 2000;202(1):173–178. doi:10.1016/S0378-5173(00)00426-9
86. You HS, Ryu S, Lee HY, Baek J-S. Enhanced antibacterial activity of multi-walled carbon nanotubes loaded with hot-melt extruded mulberry leaf silver nanoparticles. *Colloids Surf A*. 2024;699:134522. doi:10.1016/j.colsurfa.2024.134522

87. Danaei M, Dehghankhold M, Ataei S, et al. Impact of particle size and polydispersity index on the clinical applications of lipidic nanocarrier systems. *Pharmaceutics*. 2018;10(2):57. doi:10.3390/pharmaceutics10020057
88. Sharmeen S, Rahman A, Lubna MM, Salem KS, Islam R, Khan MA. Polyethylene glycol functionalized carbon nanotubes/gelatin-chitosan nanocomposite: an approach for significant drug release. *Bioact Mater*. 2018;3(3):236–244. doi:10.1016/j.bioactmat.2018.03.001
89. Selvamani V. Chapter 15 - stability studies on nanomaterials used in drugs. In: Mohapatra SS, Ranjan S, Dasgupta N, Mishra RK, Thomas S, editors. *Characterization and Biology of Nanomaterials for Drug Delivery*. Elsevier; 2019:425–444.
90. Que W, Zhou Y, Lam YL, et al. Structure and characteristics of sol-gel derived silica-titania hard optical coatings via organically modified silane precursor. *J Mater Sci Lett*. 2000;19(14):1247–1249. doi:10.1023/A:1006777513908
91. Clarkson J, Smith E, Batchelder D, Smith D, Coats A. A theoretical study of the structure and vibrations of 2,4,6-trinitrotolune. *J Mol Struct*. 2003;648:203–214. doi:10.1016/S0022-2860(03)00024-3
92. Manoharan R, Baraga JJ, Rava RP, Dasari RR, Fitzmaurice M, Feld MS. Biochemical analysis and mapping of atherosclerotic human artery using FT-IR microspectroscopy. *Atherosclerosis*. 1993;103(2):181–193. doi:10.1016/0021-9150(93)90261-R
93. Oh KI, Fiorin G, Gai F. How sensitive is the Amide I vibration of the polypeptide backbone to electric fields? *Chemphyschem*. 2015;16 (17):3595–3598. doi:10.1002/cphc.201500777
94. Cao A, Xu C, Liang J, Wu D, Wei B. X-ray diffraction characterization on the alignment degree of carbon nanotubes. *Chem Phys Lett*. 2001;344 (1):13–17. doi:10.1016/S0009-2614(01)00671-6
95. Basu S, Maji P, Ganguly J. Rapid green synthesis of silver nanoparticles by aqueous extract of seeds of Nyctanthes arbor-tristis. *Appl Nanosci*. 2016;6(1):1–5. doi:10.1007/s13204-015-0407-9
96. Chen Y, Tao J, Ezzeddine A, et al. Superior performance nanocomposites from uniformly dispersed octadecylamine functionalized multi-walled carbon nanotubes. *C*. 2015;1:58–76. doi:10.3390/c1010058
97. Xiao D, Wu C, Liang B, Jiang S, Ma J, Li Y. Outstanding ROS generation ability and the mechanism of MXene quantum dots. *J Mater Chem A*. 2024;12(45):31655–31661. doi:10.1039/D4TA05167J
98. Alfei S, Schito GC, Schito AM, Zuccari G. Reactive oxygen species (ROS)-mediated antibacterial oxidative therapies: available methods to generate ros and a novel option proposal. *Int J Mol Sci*. 2024;25(13):7182. doi:10.3390/ijms25137182
99. Shao Y, Gu W, Jiang L, Zhu Y, Gong A. Study on the visualization of pigment in haematococcus pluvialis by raman spectroscopy technique. *Sci Rep*. 2019;9(1). doi:10.1038/s41598-019-47208-2
100. Radwan B, Prabhakaran A, Rocchetti S, Matuszyk E, Keyes T, Baranska M. Uptake and anti-inflammatory effects of liposomal astaxanthin on endothelial cells tracked by Raman and fluorescence imaging. *Mikrochim Acta*. 2023;190(8). doi:10.1007/s00604-023-05888-8
101. Prime RB, Bair HE, Vyazovkin S, Gallagher PK, Riga A. Thermogravimetric analysis (TGA). *Thermal Anal Polymers*. 2009:241–317.
102. Lee M, Kim Y, Ryu H, Baeck S-H, Shim S. Effects of silane coupling agent on the mechanical and thermal properties of silica/polypropylene composites. *Polymer Korea*. 2017;41:599–609. doi:10.7317/pk.2017.41.4.599
103. Hadidi N, Mohebbi M. Anti-infective and toxicity properties of carbon based materials: graphene and functionalized carbon nanotubes. *Microorganisms*. 2022;10(12):2439. doi:10.3390/microorganisms10122439
104. Asaftei M, Lucidi M, Anton SR, et al. Antibacterial interactions of ethanol-dispersed multiwalled carbon nanotubes with Staphylococcus aureus and Pseudomonas aeruginosa. *ACS omega*. 2024;9(31):33751–33764. doi:10.1021/acsomega.4c03044
105. Mariadoss AVA, Saravanakumar K, Sathiyaseelan A, Venkatachalam K, Wang M-H. Folic acid functionalized starch encapsulated green synthesized copper oxide nanoparticles for targeted drug delivery in breast cancer therapy. *Int J Biol Macromol*. 2020;164:2073–2084. doi:10.1016/j.ijbiomac.2020.08.036
106. Saravanakumar K, Park S, Mariadoss AVA, et al. Chemical composition, antioxidant, and anti-diabetic activities of ethyl acetate fraction of Stachys riederi var. japonica (Miq.) in streptozotocin-induced type 2 diabetic mice. *Food Chem Toxicol*. 2021;155:112374. doi:10.1016/j.fct.2021.112374
107. Sathiyaseelan A, Zhang X, Wang M-H. Biosynthesis of gallic acid fabricated tellurium nanoparticles (GA-Te NPs) for enhanced antibacterial, antioxidant, and cytotoxicity applications. *Environ Res*. 2024;240:117461. doi:10.1016/j.envres.2023.117461
108. Furuta Y, Zhou Z. How do necrotic cells expose phosphatidylserine to attract their predators-What's unique and what's in common with apoptotic cells. *Front Cell Dev Biol*. 2023;11:1170551. doi:10.3389/fcell.2023.1170551
109. Dangles O. Antioxidant activity of plant phenols: chemical mechanisms and biological significance. *Cur Org Chem*. 2012;16(6):692–714. doi:10.2174/138527212799957995
110. Russo D. Flavonoids and the structure-antioxidant activity relationship. *J Pharmacogn Nat Prod*. 2018;4(1). doi:10.4172/2472-0992.1000e109
111. Aklilu E, Raman K. MCR-1 Gene Encoded Colistin-Resistant Escherichia coli in Raw Chicken Meat and Bean Sprouts in Malaysia. *International Journal of Microbiology*. 2020;2020:1–5. doi: 10.1155/2020/8853582
112. Bergdoll MS. Staphylococcal food poisoning. *Foodborne Dis*. 1990.
113. Tong SY, Davis JS, Eichenberger E, Holland TL, Fowler VG Jr. Staphylococcus aureus infections: epidemiology, pathophysiology, clinical manifestations, and management. *Clin Microbiol Rev*. 2015;28(3):603–661. doi:10.1128/CMR.00134-14
114. Krishnaraj C, Radhakrishnan S, Ramachandran R, Ramesh T, Kim B-S, Yun S-I. In vitro toxicological assessment and biosensing potential of bioinspired chitosan nanoparticles, selenium nanoparticles, chitosan/selenium nanocomposites, silver nanoparticles and chitosan/silver nanocomposites. *Chemosphere*. 2022;301:134790. doi:10.1016/j.chemosphere.2022.134790
115. Kollef MH, Shorr A, Tabak YP, Gupta V, Liu LZ, Johannes RS. Epidemiology and outcomes of health-care–associated pneumonia: results from a large us database of culture-positive pneumonia. *Chest*. 2005;128(6):3854–3862. doi:10.1378/chest.128.6.3854
116. Lee MS, Walker V, Chen LF, Sexton DJ, Anderson DJ. The epidemiology of ventilator-associated pneumonia in a network of community hospitals: a prospective multicenter study. *Infect Control Hosp Epidemiol*. 2013;34(7):657–662. doi:10.1086/670991
117. Golli A-L, Cristea OM, Zlatian O, et al. Prevalence of multidrug-resistant pathogens causing bloodstream infections in an intensive care unit. *Infect Drug Resist*. 2022;15(null):5981–5992. doi:10.2147/IDR.S383285
118. Gould IM, David MZ, Esposito S, et al. New insights into meticillin-resistant Staphylococcus aureus (MRSA) pathogenesis, treatment and resistance. *Int J Antimicrob Agents*. 2012;39(2):96–104. doi:10.1016/j.ijantimicag.2011.09.028
119. Rather AH, Singh S, Choudhary S. Antibacterial activity of Haematococcus pluvialis crude astaxanthin extract. *J Drug Delivery Ther*. 2021;11 (2–S):28–30. doi:10.22270/jddt.v11i2-S.4662

120. Haasbroek K, Yagi M, Yonei Y. Staphylococcus aureus biofilm inhibiting activity of advanced glycation endproduct crosslink breaking and glycation inhibiting compounds. *Antibiotics*. 2022;11(10):1412. doi:10.3390/antibiotics11101412
121. Ispiryan A, Atkociuniene V, Makstutiene N, et al. Correlation between Antimicrobial Activity Values and Total Phenolic Content/Antioxidant Activity in Rubus idaeus L. *Plants*. 2024; 13(4):504. doi: 10.3390/plants13040504
122. Kikuchi K, Dong Z, Shinmei Y, et al. Cytoprotective effect of astaxanthin in a model of normal intraocular pressure glaucoma. *J Ophthalmol*. 2020;2020:9539681. doi:10.1155/2020/9539681
123. Wang H-Q, Sun X-B, Xu Y-X, Zhao H, Zhu Q-Y, Zhu C-Q. Astaxanthin upregulates heme oxygenase-1 expression through ERK1/2 pathway and its protective effect against beta-amyloid-induced cytotoxicity in SH-SY5Y cells. *Brain Res*. 2010;1360:159–167. doi:10.1016/j.brainres.2010.08.100
124. Stewart JS, Lignell Å, Pettersson A, Elfving E, Soni MG. Safety assessment of astaxanthin-rich microalgae biomass: acute and subchronic toxicity studies in rats. *Food Chem Toxicol*. 2008;46(9):3030–3036. doi:10.1016/j.fct.2008.05.038
125. Takahashi J, Tsukahara H, Minato S. Toxicological studies of astaxanthin from Haematococcus pluvialis–Ames test, oral single dose and 90-days subchronic toxicity studies in rats. *J Clin Therap Med*. 2004;20(8):867–881.
126. Barros MP, Marin DP, Bolin AP *et al*. Combined astaxanthin and fish oil supplementation improves glutathione-based redox balance in rat plasma and neutrophils. *Chemico-Biological Interactions*. 2012;197(1):58–67. doi: 10.1016/j.cbi.2012.03.005
127. Zhao Y, Ye X, Xiong Z *et al*. Cancer Metabolism: The Role of ROS in DNA Damage and Induction of Apoptosis in Cancer Cells. *Metabolites*. 2023;13(7):796. doi: 10.3390/metabo13070796
128. Xuan RR, Niu TT and Chen HM. Astaxanthin blocks preeclampsia progression by suppressing oxidative stress and inflammation. *Molecular Medicine Reports*. 2016;14(3):2697–2704. doi: 10.3892/mmr.2016.5569
129. Kim S, Lee H, Lim JW, Kim H. Astaxanthin induces NADPH oxidase activation and receptor-interacting protein kinase 1-mediated necroptosis in gastric cancer AGS cells. *Mol Med Rep*. 2021;24(6):837. doi: 10.3892/mmr.2021.12477
130. Veeramuthu A. Unlocking the therapeutic potential of microalgal astaxanthin a super antioxidant in oral cancer and associated ailments. *Oral Oncol Rep*. 2024;10:100352. doi:10.1016/j.oor.2024.100352